Gonzales, Miguel Angel Calle; Kujala, Pentti

Additive manufacturing of miniature marine structures for crashworthiness verification

Published in:
Applied Ocean Research

DOI:
10.1016/j.apor.2021.102653

Published: 01/06/2021

Document Version
Publisher's PDF, also known as Version of record

Applied Ocean Research 111 (2021) 102653

Contents lists available at ScienceDirect

Applied Ocean Research

journal homepage: www.elsevier.com/locate/apor

Additive manufacturing of miniature marine structures for crashworthiness verification: A numerical revision

Miguel Angel Calle Gonzales[a,b,*], Pentti Kujala[a]

[a] Marine Technology Research Group, Department of Mechanical Engineering, Aalto University, Tietotie 1C, 02150 Espoo, Finland
[b] Engineering Modeling and Applied Social Sciences (CECS), Federal University of ABC, Av. Dos Estados, 5001, Santo André, SP, 09210-580, Brazil

ARTICLE INFO

Keywords:
Similarity
Marine structures
Finite element analysis
Thickness distortion

ABSTRACT

This work presents a revision of the structural similarity technique developed for the experimental modeling of marine structures subjected to collision, grounding or similar catastrophic events via miniature models with drastic scale reduction. This revision involved basically the inclusion of combined collapse modes to predict the mechanical behavior of structural members and the redefinition of the flow stress range. The revised technique was validated through numerical simulations of the miniature modeling of nine large-scale marine structures' experiments found in literature and here presented in the form of nine study cases. Each study case evaluates the accumulated effects of scale reduction, thickness distortion and material distortion in the miniature model as part of the similarity technique. In general, a reasonable-to-good correspondence was observed between the force and absorbed energy responses obtained from reference large-scale structures and their miniature models once brought to the same dimensional scale. Discrepancies between structural responses were quantified by evaluating the normalized root mean square error. By these means, most of the study cases presented errors below 12.5% in terms of force response and below 4.5% in terms of absorbed energy response. On the other hand, lower agreement was encountered when reproducing experiments strongly ruled by progressive buckling or crack initiation/propagation together with severe reduction scales. In these cases, better results are achieved when implementing a more accurate material failure model or by moderating the reduction scale.

1. Background

Structural aspects of ship collision and grounding accidents have been continuously investigated in the last decades due to its key relevance in marine safety studies (Soares and Garbatov, 2015; Kaminski and Rigo, 2018). With this aim, experimental collision tests in large-scale marine structures are constantly undertaken because they preserve the same construction aspects of actual structures so bringing more reliable results (Liu et al., 2018). This is why these tests are commonly used as reference to calibrate numerical/analytical modeling approaches for predicting the structural behavior of actual marine structures subjected to collision accidents (Ringsberg et al., 2018; Zhang et al., 2019; Marinatos and Samuelides, 2015). The finite element method is probably the most important tool among these numerical approaches. Despite the recent improvements in finite element codes, some aspects remain challenging to include in the modeling, for example the interaction with diverse types of cargo (Calle et al., 2017; Zhang and Suzuki, 2007), hydrodynamic effect of the surrounding water (Kim et al., 2021; Zhang and Suzuki, 2007), oil spill occurrence, ship explosion accidents (Qiankun and Gangyi, 2011; Liu et al., 2018) among others.

Most of the ship collision/grounding experiments available in literature employed reduction scales in the range of one-half to one-fifth of the actual size of marine structures so yet resulting in large-scale structures requesting huge experimental setups (Liu et al., 2018). The use of models with severe reduction scales (between 1:50 and 1:100) complicates the construction of the marine structures because original construction aspects and materials cannot be preserved or, sometimes, strong simplifications need to be adopted (Calle et al., 2017; Oshiro et al., 2017). In spite of these limitations, these simplified miniature structures were successful in reproducing coarsely the structural collapse mode of oil tanker structures subjected to collision and grounding (Calle et al., 2017) and, at the same time, used as reference to calibrate failure criteria purposely developed for ship grounding events (Calle et al., 2019).

In this respect, a new experimental technique to miniaturize marine

* Corresponding author.
E-mail address: mcallegonzales@gmail.com (M.A.C. Gonzales).

https://doi.org/10.1016/j.apor.2021.102653
Received 19 August 2020; Received in revised form 5 March 2021; Accepted 2 April 2021
Available online 19 April 2021

Table 1
Formulations for the thickness distortion technique.

Structural members by collapse mode	Proportionality of average force	$\sum F$ in original structural members	$\sum F$ in structural members with distorted thickness		Equating distortion term	Thickness distortion of each structural member
			General form	Balanced first term		
Column	I	II	III	IV	V	VI
Membrane tension	$\overline{F}_m \propto \sigma_0\ t$	$\sum_{i=1}^{I} k_{m,i}\ \sigma_{0,i}\ t_i$	$\sum_{i=1}^{I} k_{m,i}\ \sigma_0\ \left(\frac{\sigma_{0,i}}{\sigma_0}\right)\left(\eta_{t,m}\ t_i\right)$	$\left(\frac{\sigma_{0,i}}{\sigma_0}\right)\eta_{t,m}\sum_{i=1}^{I} k_{m,i}\ \sigma_0\ t_i$	$\left(\frac{\sigma_{0,i}}{\sigma_0}\right)\eta_{t,m}$	$\eta_{t,m} = \left(\frac{\sigma_{0,i}}{\sigma_0}\right)^{-1}\eta^{5/3}$
Folding	$\overline{F}_f \propto \sigma_0\ t^{5/3}$	$\sum_{j=1}^{J} k_{f,j}\ \sigma_{0,j}\ t_j^{5/3}$	$\sum_{j=1}^{J} k_{f,j}\ \sigma_0\ \left(\frac{\sigma_{0,j}}{\sigma_0}\right)\left(\eta_{t,f}\ t_j\right)^{5/3}$	$\left(\frac{\sigma_{0,j}}{\sigma_0}\right)\eta_{t,f}{}^{5/3}\sum_{j=1}^{J} k_{f,j}\ \sigma_0\ t_j{}^{5/3}$	$\left(\frac{\sigma_{0,j}}{\sigma_0}\right)\eta_{t,f}{}^{5/3}$	$\eta_{t,f} = \left(\frac{\sigma_{0,j}}{\sigma_0}\right)^{-3/5}\eta$
Tearing	$\overline{F}_t \propto \sigma_0\ t^{3/2}$	$\sum_{k=1}^{K} k_{t,k}\ \sigma_{0,k}\ t_k^{3/2}$	$\sum_{k=1}^{K} k_{t,k}\ \sigma_0\ \left(\frac{\sigma_{0,k}}{\sigma_0}\right)\left(\eta_{t,t}\ t_k\right)^{3/2}$	$\left(\frac{\sigma_{0,k}}{\sigma_0}\right)\eta_{t,k}{}^{3/2}\sum_{k=1}^{K} k_{t,k}\ \sigma_0\ t_k{}^{3/2}$	$\left(\frac{\sigma_{0,k}}{\sigma_0}\right)\eta_{t,k}{}^{3/2}$	$\eta_{t,k} = \left(\frac{\sigma_{0,k}}{\sigma_0}\right)^{-2/3}\eta^{10/9}$
Membrane tension and tearing	$\overline{F}_{m+t} \propto \sigma_0\ t^{5/4}$	$\sum_{l=1}^{L} k_{m+t,l}\ \sigma_{0,l}\ t_l^{5/4}$	$\sum_{l=1}^{L} k_{m+t,l}\ \sigma_0\ \left(\frac{\sigma_{0,l}}{\sigma_0}\right)\left(\eta_{t,m+t}\ t_l\right)^{5/4}$	$\left(\frac{\sigma_{0,l}}{\sigma_0}\right)\eta_{t,m+t}{}^{5/4}\sum_{l=1}^{L} k_{m+t,l}\ \sigma_0\ t_l{}^{5/4}$	$\left(\frac{\sigma_{0,l}}{\sigma_0}\right)\eta_{t,m+t}{}^{5/4}$	$\eta_{t,m+t} = \left(\frac{\sigma_{0,l}}{\sigma_0}\right)^{-4/5}\eta^{4/3}$
Membrane tension and folding	$\overline{F}_{m+f} \propto \sigma_0\ t^{4/3}$	$\sum_{m=1}^{M} k_{m+f,m}\ \sigma_{0,m}\ t_m{}^{4/3}$	$\sum_{m=1}^{M} k_{m+f,m}\ \sigma_0\ \left(\frac{\sigma_{0,m}}{\sigma_0}\right)\left(\eta_{t,m+f}\ t_m\right)^{4/3}$	$\left(\frac{\sigma_{0,m}}{\sigma_0}\right)\eta_{t,m+f}\sum_{m=1}^{M} k_{m+f,m}\ \sigma_0\ t_m{}^{4/3}$	$\left(\frac{\sigma_{0,m}}{\sigma_0}\right)\eta_{t,m+f}{}^{4/3}$	$\eta_{t,m+f} = \left(\frac{\sigma_{0,m}}{\sigma_0}\right)^{-3/4}\eta^{5/4}$
All	-	$\sum F$	$\sum \eta_F\ F$	$\eta_F \sum F$	η_F	$\eta_F = \eta^{5/3}$

structures, with the aim to create models to reproduce their structural responses when subjected to collision or grounding events, was proposed in recent works (Calle et al., 2020, Calle et al., 2020). This technique combines structural similarity concepts, thickness distortion of the structural members of the model and material distortion.

Through similarity hypotheses, it is possible to correlate the structural behavior of a large-scale marine structure with that of equivalent miniature model (Barenblatt, 2003). However, when a marine structure is radically scaled down, its manufacture becomes a challenge in view of the resulting extremely thin plates in the structural members (Calle et al., 2017). So, a thickness distortion correction needs to be coupled to the technique to make the miniature structure able to be built using additive manufacturing technologies consequently involving also the material modification (Mazzariol et al., 2016).

This technique was previously verified via the experimental reproduction of the structural collapse of two large-scale marine structures in miniature (Calle et al., 2020; Calle et al., 2020). Regardless of the good overall correspondence of these miniature experiments with their large-scale references, especially in terms of internal energy absorption, some aspects remained not well completely clarified. For instance, some divergencies in the force responses and in the collapse modes of some specific structural members of the miniature models are still not fully well understood.

This work presents the revised version of this similarity technique and its validation through the numerical reproduction of nine large-scale ship collision/grounding tests in miniature using drastic reduction scales (50 to 100 times). All these nine experiments are available in literature and each one is here presented in the form of study case. Initially, the revision of the similarity technique is presented in Section 2 and some basic considerations for the study cases are then described in Section 3. Nine study cases ranging from perforation tests of simple panel structures to more complex ship sections subjected to collision and grounding are presented, one by one, in Section 4. Diverse aspects extracted from all study cases are summarized and discussed in Section 5 and, finally, some conclusions are presented in Section 6.

2. Similarity technique (revised)

In this section, a revision of the similarity technique presented in previous works (Calle et al., 2020, Calle et al., 2020) is here proposed. As previously commented, this similarity technique is proposed to model experimentally the structural response of marine structures when subjected to ship collision or ship grounding accidents. The similarity technique is based on the use of scaled down replicas of marine structures built using additive manufacturing. To make possible their additive manufacture, the plate thickness of the structural members needs to be distorted/increased to printable values (Calle and Kujala, 2019). The distortion of the plate thickness depends on the collapse mode of each structural member.

Originally in this technique, the collapse modes of each structural member needed to be selected strictly among three categories (membrane tension, folding or tearing) (Calle et al., 2020; Calle et al., 2020) and, if two or more simultaneous collapse modes were expected in one structural member, only the most relevant could be adopted.

In this revised version, one or two collapse modes can be attached to each structural member. To amend this aspect, formulations for thickness distortion in structural members that undergo a combination of two collapse modes were appended to the original set. The factors to distort the thickness of each structural member according its expected collapse mode are evaluated in a similar manner as in Refs. (Calle et al., 2020; Calle et al., 2020) as better described below.

According to analytical models on structural collapse, the reaction force of a thin-walled structural member when subjected to pure membrane tension ($\overline{F}_m$) is directly proportional to its thickness, when subjected to folding ($\overline{F}_f$), to its thickness raised to 5/3, and when subjected to tearing ($\overline{F}_t$), to its thickness raised to 3/2 as thoroughly

Table 2
Factors for dimensional scaling, thickness distortion and material change.

Variable	Symbol	Scale factors	Coupled scale and thickness distortion factors	Coupled scale, thickness distortion and material distortion factors
Length	β	β	β	β
Thickness	$\eta_{t,m}$	β	$\beta\ \eta^{5/3}$	$\beta\left(\frac{\sigma_{0,i}}{\sigma_0}\right)^{-1}\eta^{5/3}$
	$\eta_{t,f}$		$\beta\ \eta$	$\beta\left(\frac{\sigma_{0,j}}{\sigma_0}\right)^{-3/5}\eta$
	$\eta_{t,t}$		$\beta\ \eta^{10/9}$	$\beta\left(\frac{\sigma_{0,k}}{\sigma_0}\right)^{-2/3}\eta^{10/9}$
	$\eta_{t,m+t}$		$\beta\ \eta^{4/5}$	$\beta\left(\frac{\sigma_{0,l}}{\sigma_0}\right)^{-4/3}\eta^{4/5}$
	$\eta_{t,m+f}$		$\beta\ \eta^{5/4}$	$\beta\left(\frac{\sigma_{0,m}}{\sigma_0}\right)^{-3/4}\eta^{5/4}$
Displacement	β_δ	β	β	β
Force	β_F	β^2	$\beta^2\ \eta^{5/3}$	$\beta_{\sigma_0}\ \beta^2\ \eta^{5/3}$
Energy	β_E	β^3	$\beta^3\ \eta^{5/3}$	$\beta_{\sigma_0}\ \beta^3\ \eta^{5/3}$

explained in Refs. (Calle et al., 2020, Calle et al., 2020). In this work are also proposed some combined collapse modes, that is, middle-ground solutions of these three basic collapse modes. So, it can be argued that when a structural member is subjected to a combination of membrane tension and tearing ($\overline{F}_{m+t}$), the reaction force can be considered directly proportional to its thickness raised to 5/4 (average of 1 and 3/2) while when subjected to a combination of membrane tension and folding ($\overline{F}_{m+f}$), to its thickness raised to 4/3 (average of 1 and 5/3). At the same time, these reaction forces are also directly proportional to the flow stress (σ_0) in all cases (flow stress defined here as the average of the yield stress and ultimate tensile strength). The reaction force of each one of the original structural members can be expressed uniquely in terms of its flow stress and its plate thickness as shown in Table 1 - column I. The reaction forces of all structural members are organized by collapse mode and summed as shown in Table 1 - column II.

The thicknesses of all structural members are distorted according each collapse mode by modifying them by a factor η_t. Then, the reaction forces of each structural member with distorted thickness can be easily expressed simply by multiplying thickness by the factor η_t as shown in Table 1 - column III. A flow stress ratio was also included to detach the influence of a different material of the structural member as shown in the column III (if all structural members have the same mechanical properties, all flow stress ratios will be equal to 1.0). These additional terms can be extracted from the summations to isolate the original forms as seen in Table 1 - column IV. To induce proportional increase in the reaction force of each structural members (and, consequently, in the total force), all terms in column V need to be equated as follows:

$$\left(\frac{\sigma_{0,i}}{\sigma_0}\right)\eta_{t,m} = \left(\frac{\sigma_{0,j}}{\sigma_0}\right){\eta_{t,f}}^{5/3} = \left(\frac{\sigma_{0,k}}{\sigma_0}\right){\eta_{t,k}}^{3/2} = \left(\frac{\sigma_{0,l}}{\sigma_0}\right){\eta_{t,m+t}}^{5/4} = \left(\frac{\sigma_{0,m}}{\sigma_0}\right){\eta_{t,m+f}}^{4/3} = \eta_F = \eta^{5/3}$$

Finally, the thickness distortion factors can be expressed as a function of η and their flow stress ratios as presented in column VI. So, the total reaction force of the whole structure is multiplied by a factor η_F ($\eta^{5/3}$) when a thickness distortion η_t is applied in all structural members according their collapse modes.

Besides, the size scaling effect on the resulting force response in miniature model is evaluated based on the traditional similarity laws as revised in Ref. (Oshiro et al., 2017).

Table 2 summarizes all the similarity factors considering three cases: a miniature model, a miniature model with thickness distortion, and a miniature model with thickness distortion and material distortion. Miniature model only takes into account the size reduction and traditional similarity law for structural analysis. The miniature model with thickness distortion also considers the thickness distortion of the structural members of the model according their collapse modes. Finally, the miniature model with thickness distortion and material distortion adds the influence of changing the original material of the structural members of the model by a unique material for all of them considering that it will be additively manufactured. where $\overline{F}_m$, $\overline{F}_f$, $\overline{F}_t$, $\overline{F}_{m+t}$ and $\overline{F}_{m+f}$ are the average force responses in structural members that undergo collapse modes of membrane tension, folding, tearing, a combined membrane tension with tearing and a combined membrane tension with folding respectively; F is the total force response; k_m, k_f, k_t, k_{m+t} and k_{m+f} are constants dependent on the structural members' geometries and constraints that undergo collapse modes of membrane tension, folding, tearing, a combined membrane tension with tearing and a combined membrane tension with folding respectively; σ_0 is the flow stress of the material; η_t is the thickness factor due to thickness distortion; η_F is the force factor due to the thickness distortion; η is the distortion factor; and i, j, k, l and m are indexes used to identify each structural member that undergoes collapse modes of membrane tension, folding, tearing, a combined membrane tension with tearing and a combined membrane tension with folding respectively.

The scale factor defined by $\beta = L_m/L_p$ relates the dimensions of the model, L_m, with the corresponding dimensions in the prototype, L_p.

The thickness distortion factor for each structural member are named according their expected collapse mode in the form $\eta_{t,m}$ (membrane tension), $\eta_{t,f}$ (folding), $\eta_{t,t}$ (tearing), $\eta_{t,m+t}$ (combined membrane tension and tearing) and $\eta_{t,m+f}$ (combined membrane tension and folding). The factor η is a common variable used to express the thickness distortion formulations.

The flow stress ratios relate the flow stress of each structural member with a reference flow stress (σ_0) with the aim to uniform the materials of all structural members of the prototype to change them all to only one material of the model (material to be used in AM). The indexes i, j, k, l, and m are used to number each structural member according their collapse mode (see Table 1).

The material factor, β_{σ_0}, is a non-dimensional factor that relates the flow stresses of the model and prototype materials in the form $\beta_{\sigma_0} = (\sigma_0)_m/(\sigma_0)_p$. However, this factor strongly depends on how this flow stress is calculated. Through the analysis of the study cases, it was concluded that this factor correlates both materials (of the prototype and the model) more appropriately when expressed as a range instead a single factor (Calle et al., 2020; Calle et al., 2020). So, the upper and lower bounds for the flow stress can be defined as:

$$\frac{\left[\sigma_{flow}^{LB}\right]_m}{\left[\sigma_{flow}^{LB}\right]_p} \leq \beta_{\sigma_0} \leq \frac{\left[\sigma_{flow}^{UB}\right]_m}{\left[\sigma_{flow}^{UB}\right]_p}$$

where

Table 3
Intermediate numerical analyses performed in each study case.

Numerical analysis	Marker	Description	Size scaling	Thickness distortion	Material distortion
XP	●	Reference experimental real-scale test	-	-	-
FEA ref	▬ (black)	FE modeling of reference real-scale test	No	No	No
FEA β	▬ (yellow)	FE modeling of miniature model	Yes	No	No
FEA β+η	▬ (orange)	FE modeling of miniature model with thickness distortion	Yes	Yes	No
FEA β+η+βσ$_0$	▬ (blue)	FE modeling of miniature model with thickness distortion and material distortion	Yes	Yes	Yes

$$\sigma_{flow}^{UB} = \sigma_{ULT} \text{ and } \sigma_{flow}^{LB} = \frac{\sigma_Y + \sigma_{ULT}}{2}$$

These upper and lower bounds for the flow stress were defined in previous works as the yield stress (σ_y) and the average of the yield stress and ultimate tensile strength ($\frac{1}{2}[\sigma_y + \sigma_{UTS}]$) respectively (Calle et al., 2020; Calle et al., 2020) based on similarity works (Oshiro et al., 2017) and past analytical works in marine structures (Liu et al., 2018). In this revised technique, these upper and lower bounds are amended to the average of the yield stress and ultimate tensile strength ($\frac{1}{2}[\sigma_y + \sigma_{UTS}]$) and the ultimate tensile strength (σ_{UTS}) respectively. As a result, this amendment in the flow stress definition made it closer to the structural behavior of the material when large plastic deformations are induced or rupture occurs.

3. Numerical analysis of study cases

In this work, the efficacy of the similarity technique is numerically verified by the miniature modeling of a set of large-scale experimental tests performed in diverse types of marine structures collected from scientific and technical literature. In short, the structural response obtained from these large-scale experimental tests were compared against the equivalent response obtained from their miniature versions. The miniature modeling of each large-scale experiment was organized in study cases.

For each study case, this evaluation comprises some intermediate numerical analyses to move from the large-scale experiment to its miniature replica. In this sense, four numerical models were proposed in each study case with the aim to gain a better understanding of all encompassed aspects as long as large-scale structures are transformed into reduced scale reproductions.

The first model (called here as FEA ref) consists in the numerical modeling of the large-scale experiment in its original size. Since numerical modeling can bring itself with an uncertainty degree of accuracy that depends on diverse factors, this first model aims to generate an original-size structural response to be used as reference for the next models.

The second model (FEA β) consists in an exact copy of the first model, but in reduced scale. All dimensions were uniformly reduced according a determined scale factor whilst preserving the same material in each structural member. The scaling factor was chosen in a way that the miniature structure could gain convenient dimensions for additive manufacturing (AM) as a single consolidated part.

The third model (FEA β+η) is similar to the second model, but the thicknesses of the structural members were also increased in such a way as to make them manufacturable by AM, i.e., the minimum plate thickness should be, at least, between 0.3 and 0.4 mm. In spite of the artificial increase of the thickness, the original material of each structural member is preserved with the aim to evaluate exclusively the thickness distortion effect in the structural response.

The fourth and last model (FEA β+η+βσ$_0$) involves both the scale reduction and thickness distortion together with the material distortion. The material distortion consists in changing the original material of all structural members to that chosen for AM. Since the miniature structure is projected to be additively manufactured and, at the same time, the new material should produce an equivalent structural response, it is essential that the new material has analogous elasto-plastic and failure behaviors when compared against traditional steel materials used in shipbuilding. For this reason, the 316L austenitic steel was chosen for additive manufacturing of the miniature models as already mechanically characterized in a previous work (Calle and Kujala, 2019).

So, the numerical validation was performed thru the miniature

Table 4
Proposal for analysis of study cases.

Case study	Description	Ref.	Experiment scale	Miniature scale	Total scale	Approx. quantity of structural members	Membrane tension collapse	Folding collapse	Tearing collapse	Rupture of structural members
1	Aalto stiffened panel perforation test	(Körgesaar et al., 2018)	1:5*	1:12	1:60	15	●			●
2	CENTEC stiffened panel indentation test	(Liu et al., 2015)	1:5	1:12	1:60	11	●			●
3	Chalmers stiffened panel crushing test	(Karlsson et al., 2009)	1:3	1:15	1:45	13	●			●
4	NMRI bulbous bow crushing test	(Yamada, 2007)	1:2	1:30	1:60	20		●		
5	TUHH bulbous bow crushing test	(Martens, 2014)	1:3	1:30	1:90	16		●		
6	ASIS web girder crushing test	(Ohtsubo et al., 1994)	1:2	1:40	1:80	44	●	●		●
7	ASIS ship bottom raking test	(Ohtsubo et al., 1994)	1:3	1:30	1:90	47	●	●	●	●
8	TNO ship collision test	(Peschmann, 2001)	1:3	1:25	1:75	64	●	●	●	●
9	NSWC ship grounding test	(Rodd, 1996)	1:5	1:20	1:100	72	●	●	●	●

* Approximate scale based on general dimensions

Table 5
Evaluation of nominal thicknesses for individual structural members of miniature stiffened panel structures

Structural member	Dominant collapse mode	Prototype thickness FEA ref (mm)	YS [FS1] (MPa)	UTS (MPa)	Average [FS2] (MPa)	FS ratio	Thickness distortion factor	Model thickness FEA β (mm)	Failure strain FEA ref FEA β	Model thickness FEA β+η (mm)	Failure strain FEA β+η	Model thickness FEA β+η+βσ_0 (mm)	Failure strain FEA β+η+βσ_0
Panel plate	Membrane	3.0	275	370.7	322.8	1.0	1.516	0.25	0.66	0.5	0.754	0.5	0.754
Stiffener	Membrane	3.0	275	370.7	322.8	1.0	1.516	0.25	0.66	0.5	0.754	0.5	0.754

modeling of large-scale experiments using these four numerical models with increasing level of complexity for each study case. Hence, Table 3 depicts the main characteristics of these four numerical models (together with the experimental reference), their abbreviated names and markers' designation to identify them in the graphs.

In sum, nine study cases were carried out to corroborate the effectiveness and limitations of the similarity technique. Each study case utilized as reference an experimental test performed in a large-scale

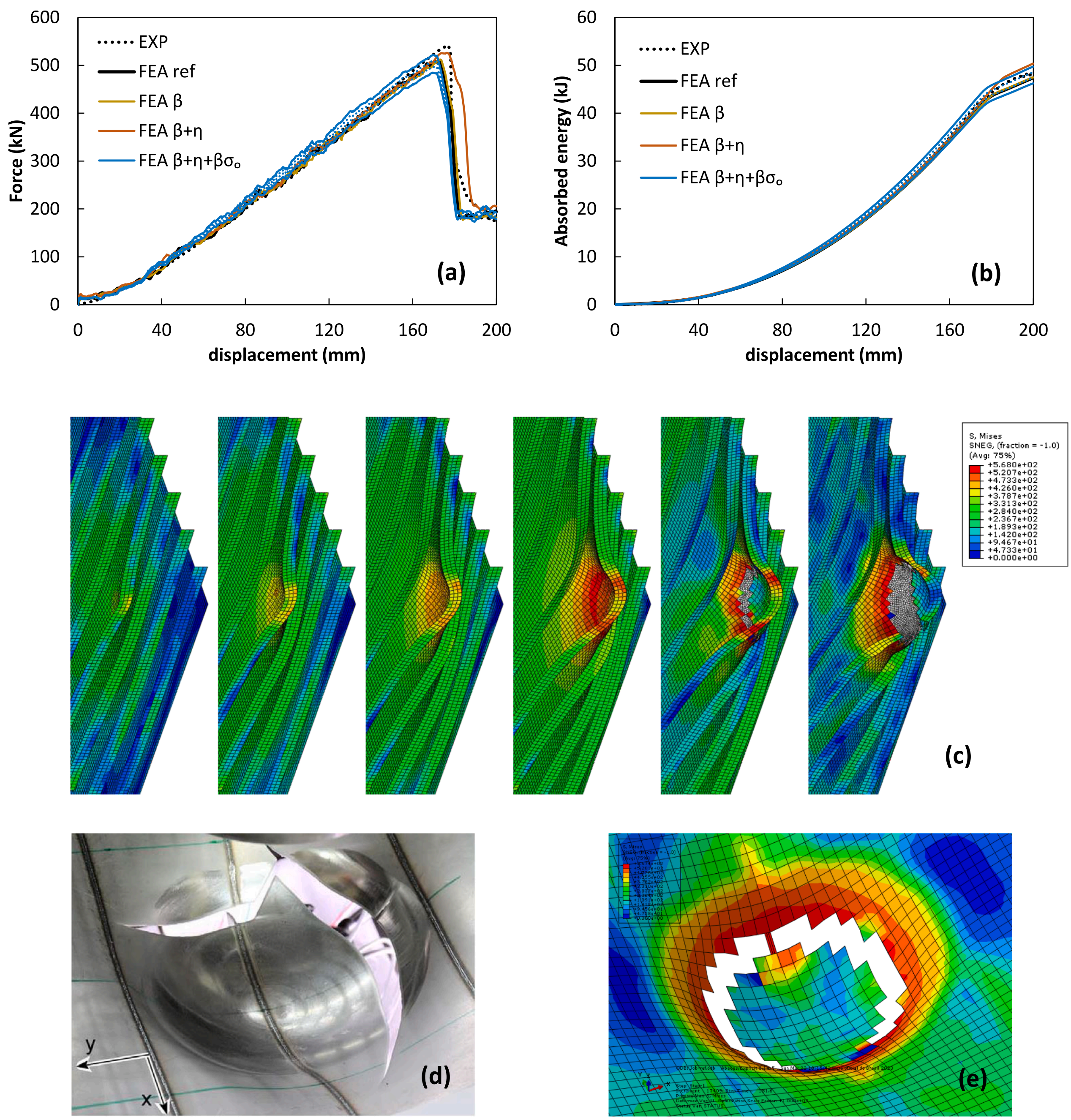

Fig. 1. Numerical modeling of perforation test of a stiffened panel structure: a) reaction force responses of real-scale and miniature tests, b) absorbed energy responses of real-scale and miniature tests, c) collapse evolution of the miniature FEA β+η+$\beta_{\sigma0}$ model, d-e) perforated plates obtained from experiment and miniature FEA β+η+$\beta_{\sigma0}$ model

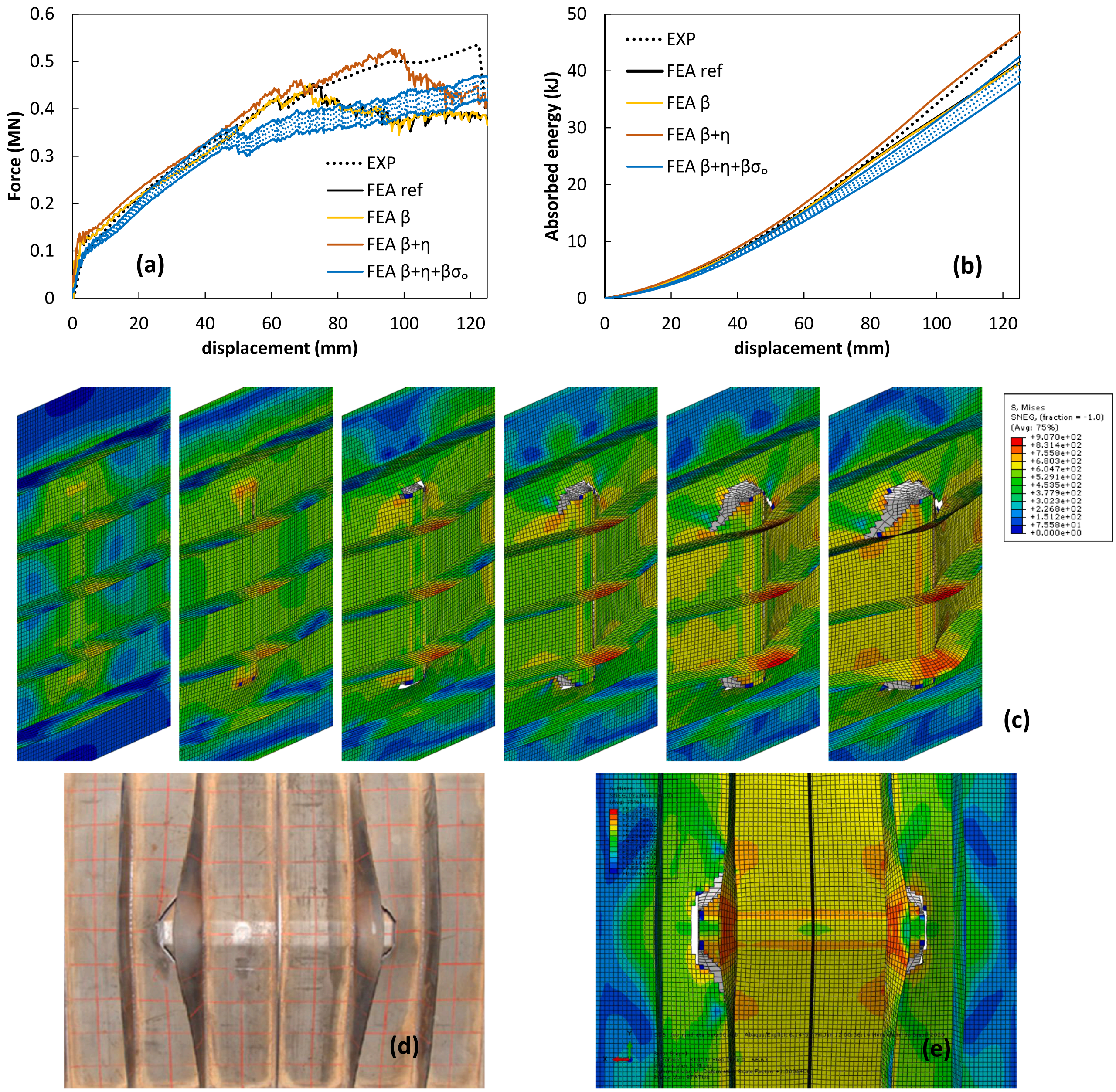

Fig. 2. Numerical modeling of indentation test of a stiffened panel structure: a) reaction force responses of real-scale and miniature tests, b) absorbed energy responses of real-scale and miniature tests, c) collapse evolution of the miniature FEA $\beta+\eta+\beta_{\sigma0}$ model, d-e) bottom view of indented plate in experiment and miniature FEA $\beta+\eta+\beta_{\sigma0}$ model

Table 6
Evaluation of nominal thicknesses for individual structural members of miniature stiffened panel structures.

Structural member	Dominant collapse mode	Prototype thickness FEA ref (mm)	YS (MPa)	UTS (MPa)	Flow stress (MPa)	FS ratio	Thickness distortion factor	Model thickness FEA β (mm)	Failure strain FEA ref FEA β	Model thickness FEA β+η (mm)	Failure strain FEA β+η	Model thickness FEA β+η+βσ$_0$ (mm)	Failure strain FEA β+η+βσ$_0$
Panel plate	Membrane	3.0	200	296	248	1.0	2.0	0.25	0.226	0.5	0.262	0.5	0.262
Stiffener	Membrane	5.0	248	368	308	1.242	2.0	0.417	-	0.833	-	0.671	-

marine structure collected from literature. The selected set of study cases aimed to encompass a wide variety of potential structural collapse modes commonly found in marine structures that undergo ship collision and ship grounding accidents, that is, membrane tension, folding, tearing or a combination of them. For each study case, the scale reduction was selected in such a manner that the total scale reduction be between 1:50 and 1:100 from its real size reference. All the study cases are listed and briefly described in Table 4.

In all study cases, the models were conceived to be run in quasi-static conditions so disregarding the influence of the strain rate on the mechanical properties of the structure as commonly assumed in diverse numerical researches in this subject (Liu et al., 2018). The Abaqus/Explicit code was wholly used for all FE models together with the mass scaling technique so to reduce the processing time of lengthy-time tests. All FE models in this work were discretized using quadrilateral shell elements (S4R) with reduced integration and five integration points through thickness which is ideal for general purpose applications (Smith, 2009). Shell elements allow modeling large thin-walled structures (such as marine structures) with fewer elements than solid elements so leading to substantial reductions in processing times (Calle and Alves, 2015). The mesh size in all reference models (FEA ref) were evaluated one by one based on reference researches (as better detailed in Supplementary material) and then its parameters were adequately extrapolated to the reduce scaled models FEA β, FEA β+η and FEA β+η+βσ$_0$.

In order to simplify the conception of the models, the failure plastic strain and its sensitivity to the element-length-to-thickness ratio (Calle and Alves, 2015) was generally employed to model the material rupture in all study cases. So, in each study case, the first model (FEA ref) was initially used to calibrate the failure plastic strain iteratively considering barely its sensitivity to the element-length-to-thickness ratio adopted from Calle et al. (Calle et al., 2019). Some study cases also required the adoption of the damage evolution option to achieve a structural response closer to the experimental reference. Therefore, all failure parameters calibrated for the FEA ref model were then properly extrapolated to the respective miniature models within the same study case (models FEA β, FEA β+η and FEA β+η+βσ$_0$).

The effectiveness of the similarity technique was evaluated quantitatively by measuring the discrepancy in the structural responses (reaction force or absorbed energy) generated by the reference model (FEA ref) and by the reduced scale model with thickness and material distortions (FEA β+η+βσ$_0$). This discrepancy is quantified by the standard deviation of the residuals (gaps between curves) measured between points of analyzed curves (root mean square error). With the aim of making comparable this error information from within diverse study cases (different scale sizes), the normalized root mean square error (NRMSE) is employed in all study cases. NRMSE formulae is detailed in Appendix.

4. Study cases

4.1. Aalto stiffened panel perforation test

With the aim to evaluate the effectiveness of FE modeling of marine structures, Kõrgesaar et al. (Kõrgesaar et al., 2018) performed perforation tests in stiffened square plates. The panel structure consists in a 3.0 mm thick square plate of 1.2 × 1.2 m stiffened by nine flat strips equally spaced. The stiffened panel was screw-mounted in a supporting base (with a 0.96 × 0.96 m hollow) and hydraulically perforated in its center point by a spherical rigid indenter. The experimental test presented a reasonable amount of plastic deformation as membrane tension in the middle area of the square plate before the abrupt crack occurrence. A significative fall in the force level occurred as a consequence of the plate rupture. At the same time, the stiffening strips underwent tension stretching together with the plate deformation. For this reason, the collapse of all structural members is assumed as membrane tension as depicted in Table 5.

A general reduction scale of 1:12 was used for all miniature models. All in all, the force and absorbed energy responses obtained from the FEA β, FEA β+η or FEA β+η+βσ0 models attained a good agreement to that obtained from FEA ref model when brought to the same dimensional scale (NRMSE = 3.03% in force and NRMSE = 1.3% in absorbed energy) as shown in Fig. 1. Just a slight difference of 4.1% in the maximum penetration before plate rupture was observed when plate thickness is distorted (FEA β+η model), but this difference was reverted when material model is modified (FEA β+η+βσ0 model).

Table 7
Evaluation of nominal thicknesses for individual structural members of miniature stiffened panel structures.

Structural member	Dominant collapse mode	Prototype thickness FEA ref (mm)	YS [FS1] (MPa)	UTS (MPa)	Flow stress (MPa)	FS ratio	Thickness distortion factor	Model thickness FEA β (mm)	Failure strain FEA ref FEA β	Model thickness FEA β+η (mm)	Failure strain FEA β+η	Model thickness FEA β+η+βσ$_0$ (mm)	Failure strain FEA β+η+βσ$_0$
Upper plate	Membrane	5	282	395.5	338.7	1.0	3.175	0.333	0.190	1.058	0.236	1.058	0.236
Lower plate	Membrane	5	282	395.5	338.7	1.0	3.175	0.333	0.190	1.058	0.236	1.058	0.236
Vertical plate	Folding	3	282	395.5	338.7	1.0	2.00	0.200	0.170	0.40	0.197	0.40	0.197
L-profile	Folding	4	282	395.5	338.7	1.0	2.00	0.267	0.181	0.533	0.209	0.533	0.209
T-beam web	Folding	3	282	395.5	338.7	1.0	2.00	0.200	0.170	0.40	0.197	0.40	0.197
T-beam flange	Folding	5	282	395.5	338.7	1.0	2.00	0.333	0.190	0.667	0.217	0.667	0.217

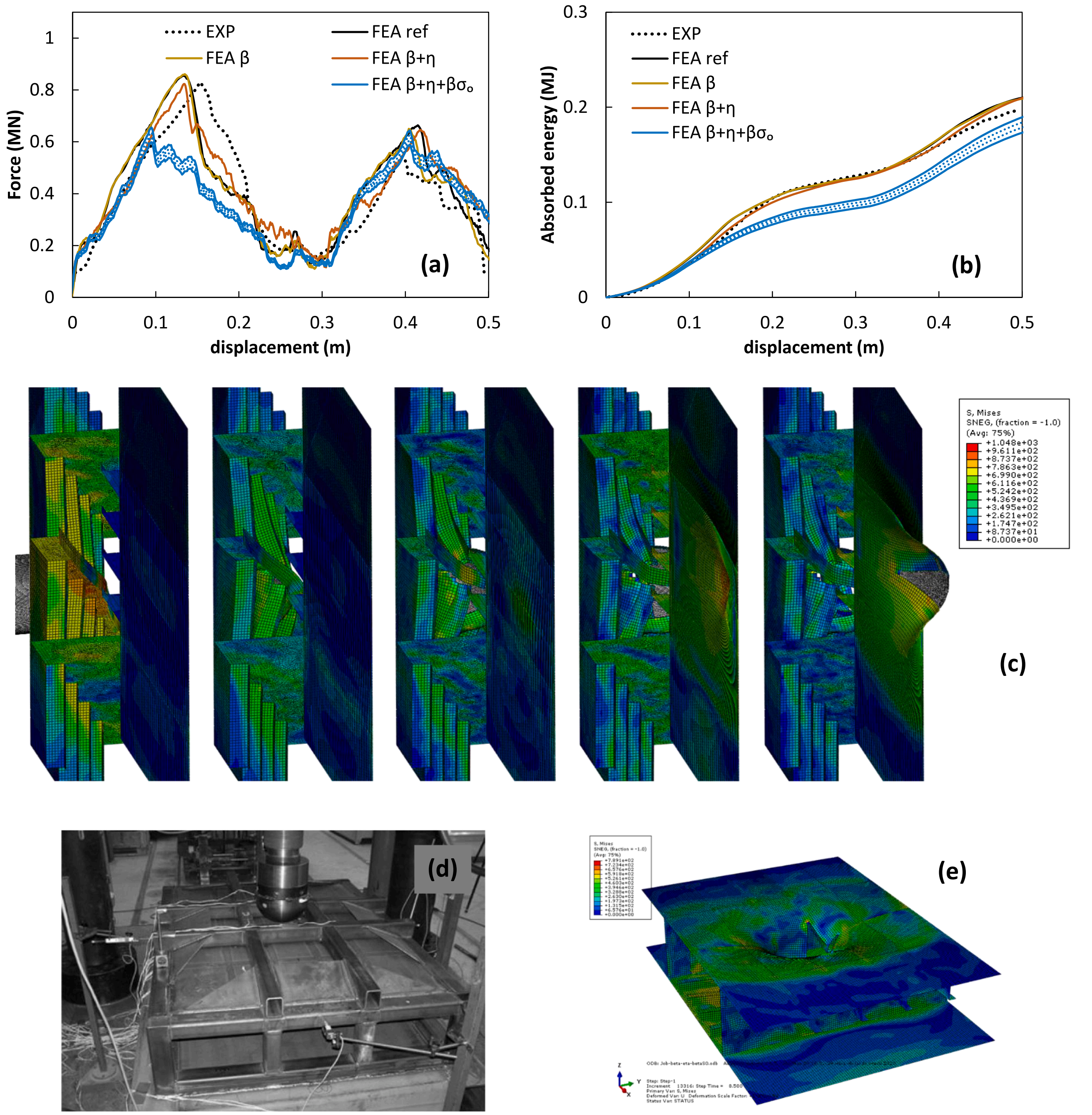

Fig. 3. Numerical modeling of crushing test of stiffened panel: a) reaction force responses of real-scale and miniature tests, b) absorbed energy responses of real-scale and miniature tests, c) collapse evolution of the miniature FEA $\beta+\eta+\beta_{\sigma 0}$ model, d) experimental setup and e) collapsed panel obtained from miniature FEA $\beta+\eta+\beta_{\sigma 0}$ model

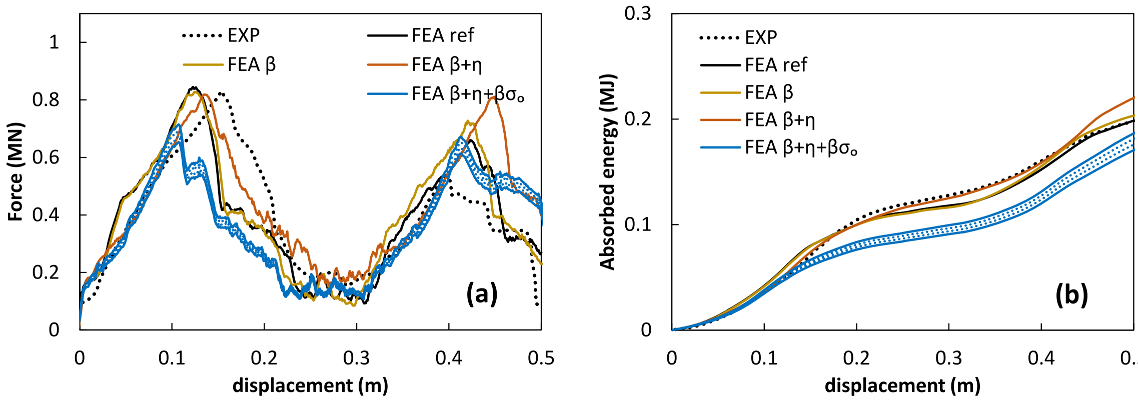

Fig. 4. Numerical modeling of crushing test of stiffened panel using a stress triaxiality-based failure criterion: a) reaction force responses of real-scale and miniature tests, b) absorbed energy responses of real-scale and miniature tests

4.2. CENTEC stiffened panel indentation test

With the aim to validate a simplified analytical method to examine the energy absorbing mechanisms of stiffened plate specimens, Liu et al. (Liu et al., 2015; Liu and Soares, 2016) performed quasi-static punching tests in stiffened rectangular plates. The panel structure consists in a 3.0 mm thick rectangular plate of 0.96 × 0.8 m stiffened by five 5.0 mm thick flat strips equally spaced. The specimens were conceived to represent a one fifth scaled tanker side panel structure. The experimental setup included a stiff frame to fix the specimen and fully constraint all its perimeter. The stiffened plate was centrally punched by a rigid flat edge indenter moved with a hydraulic cylinder at a rate of 10 mm/min.

The experimental test presented a moderate amount of plastic deformation as membrane tension before crack initiation. Two cracks initiated simultaneously in the plate areas in direct contact with the indenter corners because of the flat geometry of the indenter. The cracks' initiation was followed by a gradual fall of the force level since the both cracks grew slowly, but not evolved to a complete rupture of the stiffened plate. As observed in Fig. 2, it was not possible to reproduce completely the force response after the crack initiation in the FEA ref model (Liu et al., 2015). The FEA β model considered a uniform scale reduction of 1:15 and the force response attained a good agreement with that of the reference. To be coherent with the previous study case, the collapse of all structural members is also assumed as membrane tension as shown in Table 6. However, the force response obtained from FEA β+η and FEA β+η+βσ0 models diverged moderately from that of the reference model (NRMSE = 7.72%) with an accentuated discrepancy in the crack initiation moment (25% difference in displacement point where crack initiated) as seen in Fig. 2. In spite of this, an acceptable correlation was found in terms of absorbed energy (NRMSE = 3.37%).

4.3. Chalmers stiffened panel crushing test

Karlsson et al. (*Ringsberg et al., 2018*; *Karlsson et al., 2009*) performed a quasi-static perforation test in a double plate panel using bulb rigid indenter with the aim to calibrate the finite element procedure to model ship collision events. The panel structure was designed to represent an actual side shell structure scaled down by a factor of 3. The main dimensions of the panel are 1.5 × 1.09 m with a height of 0.3 m. The panel basically consists in outer and inner side shells, web plates to carry axial loading and L-profiles stiffeners to carry lateral loading, Table 7. The test was executed in a press machine that projected the bulb indenter perpendicularly, at a velocity of 4 mm/s, to the center of the panel surface. A reinforcing frame was built around the panel structure to create clamped boundary conditions.

An acceptable agreement was obtained between the experiment (EXP) and the reference model (FEA ref) in the replication of the overall structural response likewise other research efforts (Ringsberg et al., 2018). Both miniature models, FEA β and FEA β+η models (reduction scale of 1:15), also achieved a good correspondence with the FEA ref model when compared in the same size scale. However, when modifying the structure's material (FEA β+η+βσ0 model), an early fall in the first peak force (24% fall) was provoked so prejudicing drastically (from this point forward) the compatibility with the reference in terms of force response (NRMSE = 12.7%) and absorbed energy response (NRMSE = 11.5%) so spreading a gap in energy level around 25 kJ as seen in Fig. 3. This early fall in the peak force (in the FEA β+η+βσ0 model) occurs due to the premature crack formation in the T-beam web below the outer plate during its plastic stretching. This premature crack formation is caused by numerical inaccuracies related to the strain-based failure criterion as the crack formation got retarded when a stress triaxiality-based failure criterion is implemented instead as seen in Fig. 4. Despite that, the error in force response remained almost the same (NRMSE = 12.5%) above, but the discrepancy in the absorbed energy was slightly reduced to NRMSE = 9.75%. In this analysis, the stress triaxiality-based failure criterion was calibrated using a different material (Calle et al., 2019), a more precise calibration was not feasible since original data is not available.

4.4. NMRI bulbous bow crushing test

To investigate the collapse mechanism of various bulbous bow configurations, experimental crush tests in buffer bow models were carried out by Yamada (Yamada, 2007; Endo et al., 2002; Yamada and Pedersen, 2008). The BC-G bow is a reproduction in almost half scale of a real bulbous bow of an actual VLCC tanker (2.48 m height and 2.9 m diameter of the base). The bow has a conical body with a spherical nose geometry and its internal structure consists basically in two crossing web structures together with five transversal stiffening rings. A rigid plate

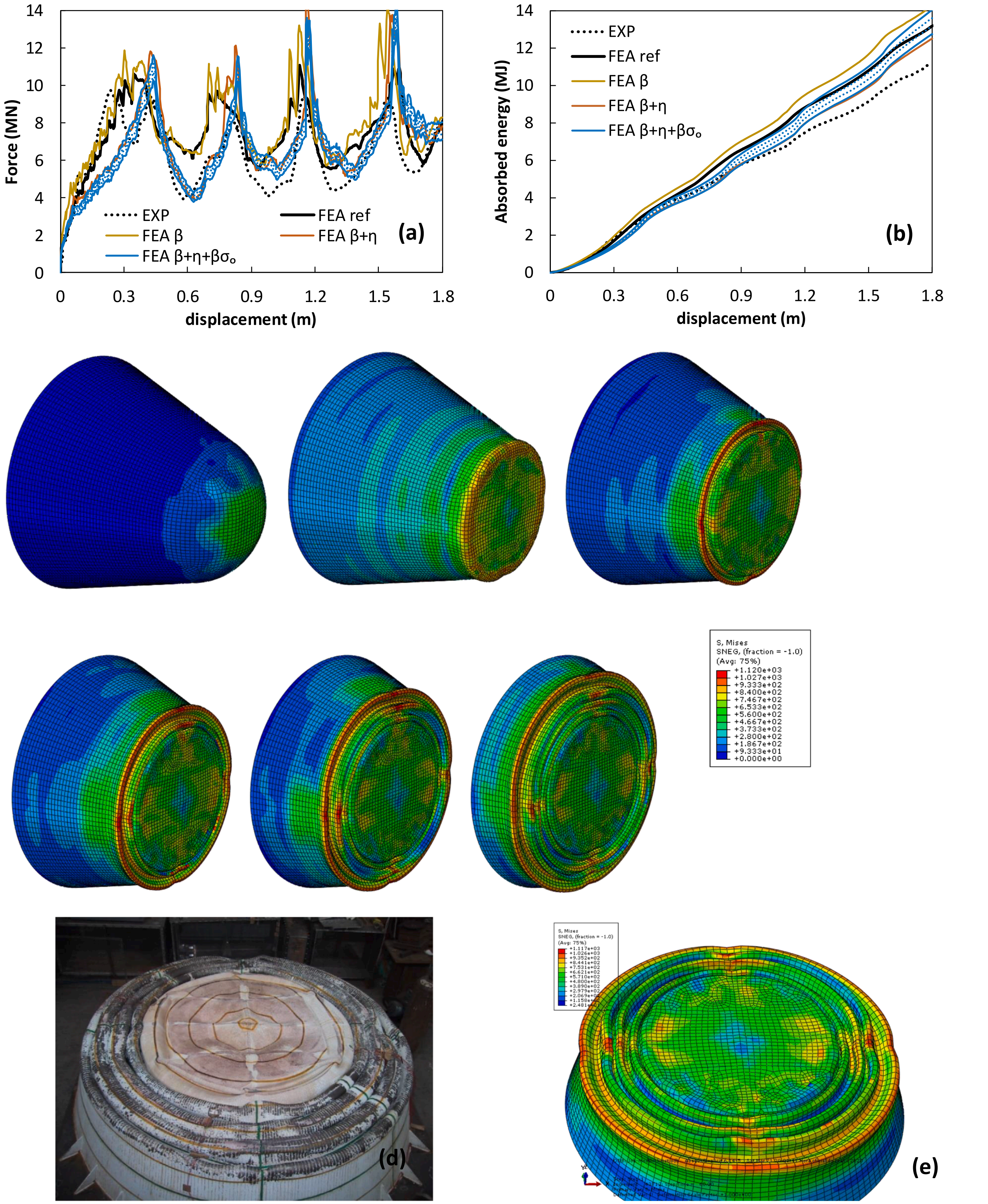

Fig. 5. Numerical modeling of crushing test of bulbous bow structure: a) reaction force responses of real-scale and miniature tests, b) absorbed energy responses of real-scale and miniature tests, c) collapse evolution of the miniature FEA $\beta+\eta+\beta_{\sigma0}$ model, d-e) crushed bulbous bow obtained from experiment and miniature FEA $\beta+\eta+\beta_{\sigma0}$ model

Table 8
Evaluation of nominal thicknesses for individual structural members of miniature bulbous bow structures.

Structural member	Dominant collapse mode	Prototype thickness FEA ref (mm)	YS [FS1] (MPa)	UTS (MPa)	Average [FS2] (MPa)	FS ratio	Thickness distortion factor	Model thickness FEA β (mm)	Failure strain FEA ref FEA β	Model thickness FEA β+η (mm)	Failure strain FEA β+η	Model thickness FEA β+η+βσ$_0$ (mm)	Failure strain FEA β+η+βσ$_0$
Outer shell	Folding	10	361	451	406	1.481	1.50	0.333	-	0.74	-	0.937	-
Transversal ring web	Folding	7	226	322	274	1.0	2.22	0.233	-	0.518	-	0.518	-
Transversal ring frame	Folding	10	361	451	406	1.481	1.50	0.333	-	0.74	-	0.937	-
Centerline web	Folding	7	226	322	274	1.0	2.22	0.233	-	0.518	-	0.518	-
Horizontal web	Folding	7	226	322	274	1.0	2.22	0.233	-	0.518	-	0.518	-

was hydraulically moved to compress the bow structure.

The structural collapse of the BC-G bulbous bow consisted in a progressive inward folding of each section as the sectional diameter expanded with test penetration as shown in Fig. 5. So, the collapse mode of all structural members is assumed as folding as described in Table 8. The reference model (FEA ref) replicated reasonably all experimental force peaks in magnitude and position. The FEA β model also achieved a good correspondence with the FEA ref model when compared in the same size scale. But when using a thickness distortion (FEA β+η and FEA β+η+βσ0 models), a slight shift in the positions of the force peaks (about 20% shift) as well as an alteration of their shapes (30% reduction in force peak breadths) are induced so leading to an error of NRMSE = 16.2% when FEA ref and FEA β+η+βσ0 are compared (Fig. 5). In spite of that, there is an evident compatibility in the resulting collapse mode of the whole bow structure and in the absorbed energy (NRMSE = 2.8%).

4.5. TUHH bulbous bow crushing test

Crushing tests in deformable bulbous bows driven against a rigid flat plate were performed by Martens (Martens, 2014, Tautz et al., 2010). The VV1 bow structure consists in a cylindrical with a bulge nose construction of 1.8 m height and 0.813 m diameter. The bow was provided with a central longitudinal bulkhead, stringers and ring stiffeners equally spaced, Table 9. The complete bow structure was made of grade-A steel plate (5.0 mm thick). A hydraulic system was employed to crush the bow structure vertically against a flat rigid plate. The experimental collapse of the VV1 bow exhibited a progressive folding collapse of the bow structure starting from the bow bulge as also seen in Fig. 5. In view of this, all structural members are assumed to collapse by folding mechanism as described in Table 9.

During the numerical modeling of the reference test (FEA ref), it was necessary to adopt a failure criterion with damage evolution to allow modeling the small cracks occurrence in folded regions without the sudden deletion of elements after their rupture. These small cracks had a significant role in the configuration of the structural force response. By doing so, it was possible to numerically reproduce the oscillating force peaks at the same position as shown in Fig. 6. All the miniature models were created considering a reduction scale of 1:30 and its structural response was nearly identical to the reference model once brought to the same size scale. However, the thickness distortion in the FEA β+η and FEA β+η+βσ0 models ended up modifying drastically the force peak positions mainly due to slight alterations in the folding pattern and, consequently, in the absorbed energy. As a result, the discrepancy between FEA ref and FEA β+η+βσ0 resulted in NRMSE = 20.1% in terms of crushing force response and in NRMSE = 7.96% in terms of absorbed energy response. A folding pattern closer to that obtained from the experimental reference can be induced in the model by presetting a warping in the external shell of the bow model, analogous to the expected folding pattern, considering a warping amplitude of about 50% of the plate thickness. In spite of reproducing the reference collapse mode successfully (and reducing the error in reaction force response to NRMSE = 14.7%), the error in the absorbed energy slightly increased (NRMSE = 9.86%) as can be seen in Fig. 7. On the other hand, a better reproduction of the collapse mode, force level and absorbed energy are achieved when employing not so drastic reducing scales as verified when using instead a 1:15 scale model (without relying on a preset warping in the structure geometry) so reducing the divergence between FEA ref and FEA β+η+βσ0 models in terms of reaction force (NRMSE = 10.9%) and, practically, eliminating the discrepancy in absorbed energy

Table 9
Evaluation of nominal thicknesses for individual structural members of miniature bulbous bow structures.

Structural member	Dominant collapse mode	Prototype thickness FEA ref (mm)	YS [FS1] (MPa)	UTS (MPa)	Average [FS2] (MPa)	FS ratio	Thickness distortion factor	Model thickness FEA β (mm)	Failure strain FEA ref FEA β	Model thickness FEA $\beta+\eta$ (mm)	Failure strain FEA $\beta+\eta$	Model thickness FEA $\beta+\eta+\beta\sigma_0$ (mm)	Failure strain FEA $\beta+\eta+\beta\sigma_0$
Outer shell	Folding	5.0	325	466.2	395.6	1.0	3.0	0.167	0.286	0.5	0.362	0.5	0.362
Bulkhead	Folding	5.0	325	466.2	395.6	1.0	3.0	0.167	0.286	0.5	0.362	0.5	0.362
Stringer	Folding	5.0	325	466.2	395.6	1.0	3.0	0.167	0.286	0.5	0.362	0.5	0.362
Rings	Folding	5.0	325	466.2	395.6	1.0	3.0	0.167	0.286	0.5	0.362	0.5	0.362

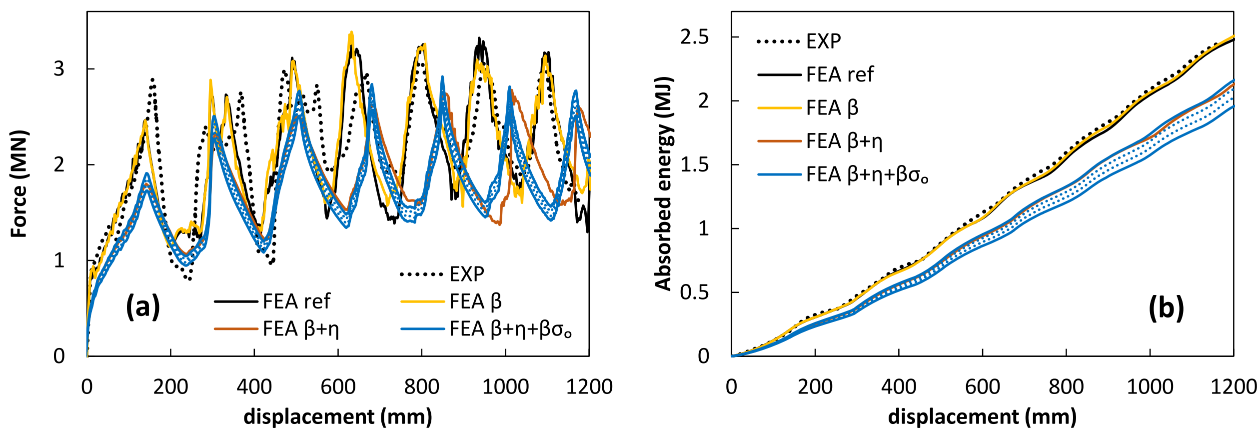

Fig. 6. Numerical modeling of crushing test of bow structure: a) reaction force responses of real-scale and miniature tests, b) absorbed energy responses of real-scale and miniature tests

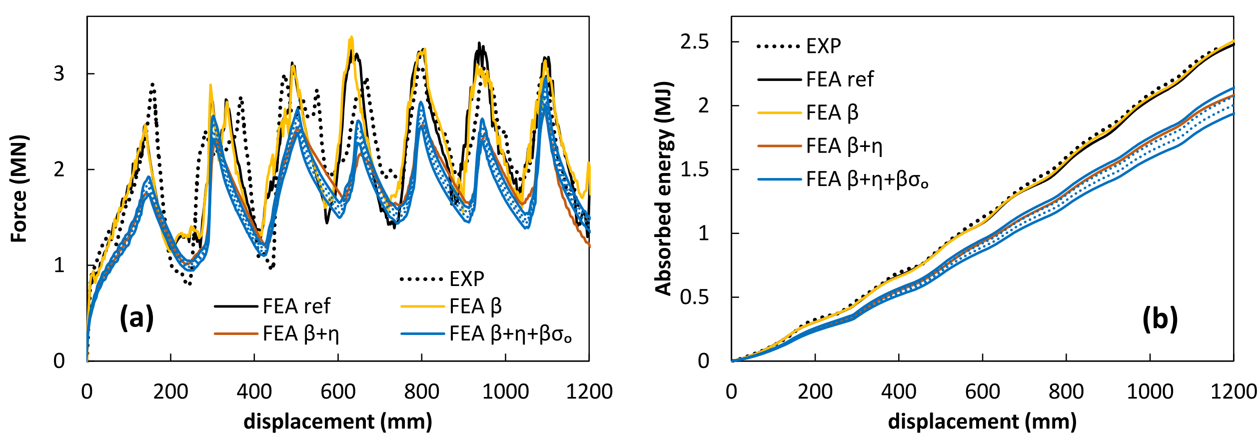

Fig. 7. Numerical modeling of crushing test of bow structure considering a preset collapse mode in the model: a) reaction force responses of real-scale and miniature tests, b) absorbed energy responses of real-scale and miniature tests

(NRMSE = 2.02%) as shown in Fig. 8.

4.6. ASIS web girder crushing test

Collision tests in large-scale marine structures were performed by the Association for Structural Improvement of Shipbuilding Industry (ASIS) (Ohtsubo et al., 1994). One of these tests, a quasi-static crushing test of a web girder structure built in a half scale of an actual structure was here reproduced. This structure corresponds to a section of a VLCC tanker's side structure which is crushed by a rigid bow-like indenter in midspan. The main dimensions of the web girder structure are 6.0 m length × 1.6 m height. Both the lateral ends and the bottom plate were attached to rigid supporting structures by welding. The crushing experiment provoked a longitudinal stretching of the side shell structural member during the direct contact with the rigid indenter while the rest of the structural members underwent folding and buckling. For these reasons,

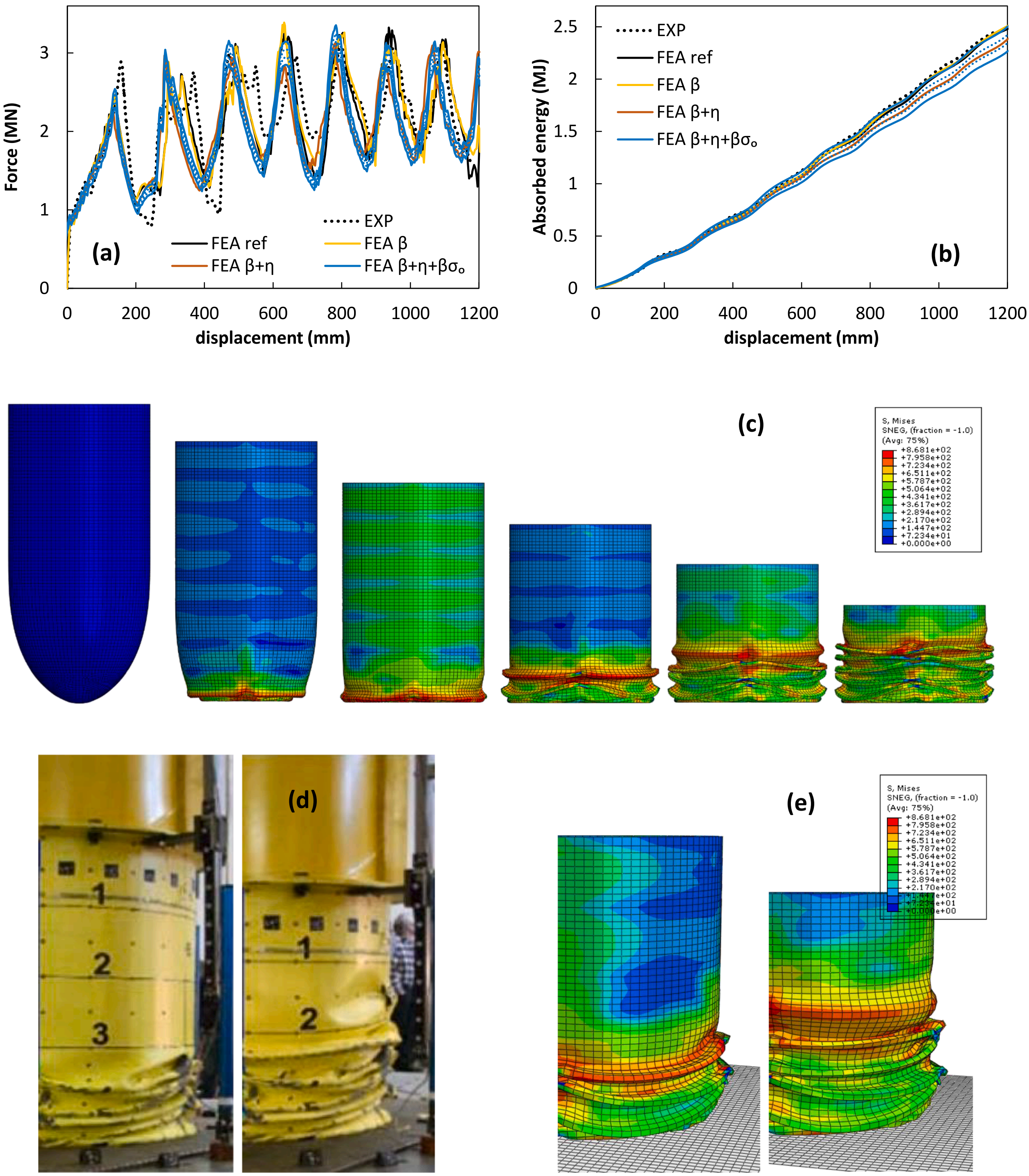

Fig. 8. Numerical modeling of crushing test of bow structure considering a 1:15 scale reduction: a) reaction force responses of real-scale and miniature tests, b) absorbed energy responses of real-scale and miniature tests, c) collapse evolution of the miniature FEA β+η+βσ0 model, d-e) two partially crushed bow configurations obtained from experiment and miniature FEA β+η+βσ0 model

Table 10
Evaluation of nominal thicknesses for individual structural members of miniature web girder structures.

Structural member	Dominant collapse mode	Prototype thickness FEA ref (mm)	YS [FS1] (MPa)	UTS (MPa)	Average [FS2] (MPa)	FS ratio	Thickness distortion factor	Model thickness FEA β (mm)	Failure strain FEA ref FEA β	Model thickness FEA β+η (mm)	Failure strain FEA β+η	Model thickness FEA β+η+βσ$_0$ (mm)	Failure strain FEA β+η+βσ$_0$
Side shell	Membrane	10	324	442.1	383.1	1.002	5.741	0.25	0.357	1.438	0.487	1.435	0.486
Stringer deck	Folding	7	314	450.7	382.3	1.0	2.857	0.175	0.33	0.5	0.408	0.5	0.408
Transversal web	Folding	8	324	452.1	388	1.015	2.832	0.2	0.34	0.571	0.418	0.566	0.417
Stiffener of stringer deck	Folding	7	314	450.7	382.3	1.0	2.857	0.175	0.33	0.5	0.408	0.5	0.408
Stiffener of transversal web	Folding	7	314	450.7	382.3	1.0	2.857	0.175	0.33	0.5	0.408	0.5	0.408

the collapse mode chosen for the side shell structure was membrane tension and folding for the other structures as listed in Table 10.

This experiment was first numerically reproduced in the real size (FEA ref) where the collapse modes of all structural members seemed to be properly simulated. Furthermore, the FEA β model also attained good correspondence with the FEA ref model when brought to an equivalent scale. The FEA β+η and FEA β+η+βσ0 models also achieved a good agreement in terms of absorbed energy, but with some slight divergences in the structural force response (rise in peak force of about 5.8% just before rupture initiation) as show in Figure 9. This higher value of the initial peak force was produced in these miniature models (as also observed in the miniature experiment (Calle et al., 2020)) which was probably caused by the thickness distortion that ended up altering the mechanical conditions to trigger buckling, i.e., to initiate the folding process. In spite of this, a reasonable compatibility in terms of crushing force response (NRMSE = 12.4%) and a good compatibility in terms of absorbed energy response (NRMSE = 2%) are obtained when comparing both FEA ref and FEA β+η+βσ0 models.

4.7. ASIS ship bottom raking test

This experimental test was also part of the set of tests in large-scale marine structures performed by the Association for Structural Improvement of Shipbuilding Industry (ASIS) (*Ohtsubo et al., 1994*). A quasi-static raking test of a bottom structure of a VLCC tanker was performed in a 1:3 scale of an actual structure. The test consists basically in a ship bottom structure laterally torn by a sharp rigid indenter. The aim of this experiment was to reproduce experimentally the structural collapse of ship bottom structures subjected to a ship grounding accident. The bottom structure consists in a single outer shell structure and a transversal web, both reinforced with longitudinal stiffeners. The general dimensions of the structure are 4.5 m width × 2.0 m height (*Törnqvist, 2003*). Analogously to the web girder structure, the lateral ends and bottom of the ship bottom structure were also constrained to rigid supporting structures by welding.

The outer shell was progressively torn by the sharp edge of the indenter so showing minor material stretching before rupture. A tearing collapse mode was chosen for the outer shell as depicted in Table 11. On the other hand, the transversal web was also hit by the sharp edge of the indenter, but this structural member showed a significant amount of stretching before rupture occurrence. A combination of membrane tension and tearing collapse modes was adopted for the transversal web structural member (Table 11) in view of a better correspondence achieved for miniature models with thickness distortion, i.e., FEA β+η and FEA β+η+βσ0 models. The folding collapse mode was chosen for the rest of the structural members related with structural stiffening. In spite of these considerations, an evident lack of compatibility in the force level (NRMSE = 14.6%) was observed when the rigid indenter starts touching the transversal web member as seen in Fig. 10. As a consequence, a reasonable correspondence in terms of absorbed energy (NRMSE = 10%) was also observed between FEA ref and FEA β+η+βσ0 models' responses. One of the potential sources of error is the inaccuracy of the plastic strain-based failure criterion to model properly the pure tearing process (bottom shell) since this phenomenon is highly dependent on the stress triaxiality (*Calle et al., 2019*). So, when stress triaxiality dependence is introduced into the failure criterion, the discrepancy in the force response remains nearly the same (NRMSE = 13.3%) while the discrepancy in the absorbed energy response is strongly reduced (NRMSE = 2.63%) as seen in Fig. 11. Despite that numerical improvement, the lack of compatibility in force response persists at the moment when rigid indenter touches the transversal web member.

4.8. TNO ship collision test

Ship collision experiments, in 1:3 scale, were carried out by the Organization for Applied Scientific Research (TNO) in Netherlands

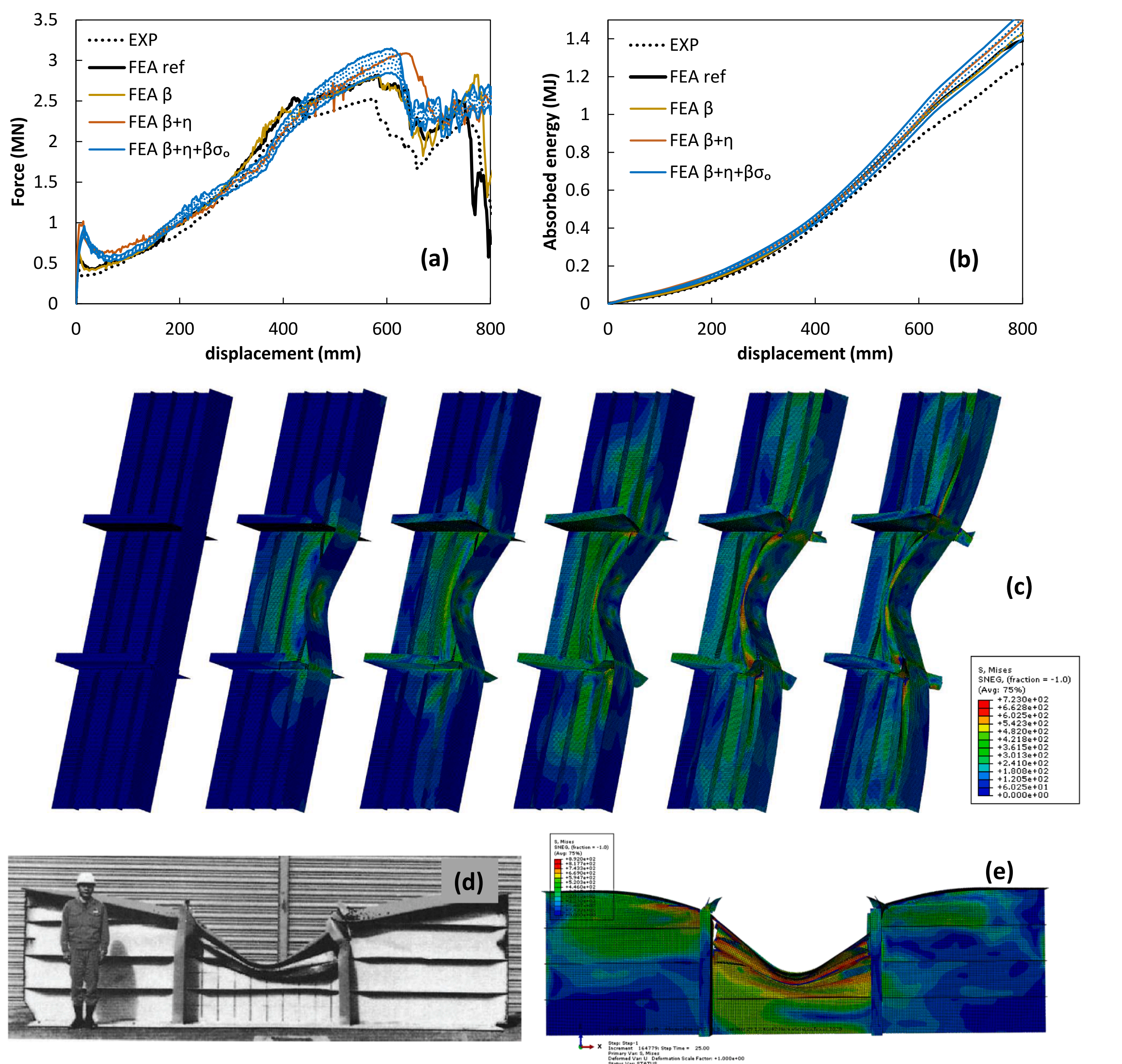

Fig. 9. Numerical modeling of quasi-static crushing test of web girder structure: a) reaction force response of real-scale and miniature tests, b) absorbed energy responses of real-scale and miniature tests, c) collapse evolution of the miniature FEA β+η+βσ0 model, d-e) crushed web girder obtained from experiment and miniature FEA β+η+$\beta_{\sigma 0}$ model

Table 11
Evaluation of nominal thicknesses for individual structural members of miniature ship bottom structures.

Structural member	Dominant collapse mode	Prototype thickness FEA ref (mm)	YS [FS1] (MPa)	UTS (MPa)	Average [FS2] (MPa)	FS ratio	Thickness distortion factor	Model thickness FEA β (mm)	Failure strain FEA ref FEA β	Model thickness FEA β+η (mm)	Failure strain FEA β+η	Model thickness FEA β+η+βσ$_0$ (mm)	Failure strain FEA β+η+βσ$_0$
Bottom shell	Tearing	7.0	295	402.1	348.6	0.964	2.49	0.233	0.24	0.56	0.29	0.574	0.291
Longitudinal stiffener web	Folding	6.0	315	408	361.5	1.0	2.2	0.2	0.231	0.44	0.276	0.44	0.276
Longitudinal stiffener flange	Folding	9.0	295	435.6	365.3	1.011	2.177	0.3	0.254	0.66	0.299	0.656	0.299
Transversal ring web	Tearing and Membrane	5.0	315	408	361.5	1.0	2.401	0.166	0.221	0.477	0.281	0.477	0.281
Transversal ring stiffener	Folding	4.5	315	408	361.5	1.0	2.2	0.15	0.215	0.33	0.26	0.33	0.26
Transversal ring face	Tearing and Membrane	9.0	295	435.6	365.3	1.011	2.376	0.3	0.254	0.858	0.314	0.851	0.314

within the scope of an international cooperation to gain technological basis for further researches to enhance collision safety (*Peschmann, 2001*; *Lehmann and Peschmann, 2002*). The perpendicular ship collision test, carried out in waters, was used as reference in this study case. Two inland waterway vessels (80 m length each) were adapted for these tests. The striking ship was assembled with a rigid bulbous bow and a measuring system to acquire the contact force during the collision. The struck ship was adapted with a lateral frame to accommodate a double-plate hull of 4.2 m height × 7.5 m length. The velocity of the striking ship was 2.5 m/s while the struck ship stayed still. Aiming to reproduce rigorously the experiment, the impact point of the bow was shifted from the center of the double-plate hull in {Z = -0.27 m; X = 0.45 m} and the collision angle deviated 3° from perpendicularity.

The resulting force response presented two peak values, the first related with the rupture of the outer plate and, the second, with the inner one. An increase of the force level also occurred after the outer plate rupture and as long as the test progresses, Fig. 12. Both outer and inner plates underwent membrane tension while stretched during the contact with the rigid bow, but, once the crack initiated, further bow penetration provoked the tearing of the cracks' plate. For this reason, and taking into account the better results obtained in models with thickness distortion (FEA β+η and FEA β+η+βσ0 models), the collapse mode of both outer and inner shells is chosen as a combination of membrane tension and tearing as shown in Table 12. The collapse mode for the rest of the structural members was chosen as folding. Having regard to all these considerations, both FEA β+η and FEA β+η+βσ0 models showed a reasonable success in modeling the force and absorbed energy responses as seen in Fig. 12. When comparing the FEA ref and FEA β+η+βσ0 models' responses, barely a slight difference of about 9% was detected in the magnitude of the second peak force while no difference was detected in the first force peak so resulting in reasonable-to-good correspondence in terms of force reaction (NRMSE = 6.77%). It ended up also generating a small difference in the absorbed energy responses (NRMSE = 4.49%).

4.9. NSWC ship grounding test

Ship grounding experiments were conducted by the Naval Surface Warfare Center (NSWC) and reported by Rodd (*Rodd, 1996*). These tests aimed to simulate experimentally the grounding of a ship bottom structure when torn by a pinnacle rock. The ship bottom structures were conceived to correspond to that of an oil tanker of about 30,000 to 40, 000 DWT, but built in a scale of 1:5. The experimental setup consisted in the ship bottom mounted to a railway car of 223 ton that run down a hill to gain kinetic energy to finally run over an artificial rock. The reaction contact forces applied to the rock during the test were experimentally measured in vertical and horizontal directions. The general dimensions of the ship bottom structure are 7.2 m length × 2.54 m width and a height of about 0.4 m. The inclination of the sample structure to the horizontal is so, that the rock tip starts penetrating the outer shell and ends penetrating the inner shell so ensuring the tearing rupture of both shells.

The force response presented a progressive and subtle increase as long as the rock tip penetrates the shells (Simonsen, 1997; Simonsen, 1997). Following the procedure used in previous study cases, this experiment was numerically reproduced in the reference model (FEA ref) attaining good correspondence in force response, Fig. 13. Similarly, its exact miniature version in 1:20 scale, the FEA β model, also achieved a good agreement the FEA ref model when brought to an equivalent scale. On the other hand, the force responses obtained with the models with thickness distortion (FEA β+η and FEA β+η+βσ0 models) only showed good correspondence with the reference model (as seen in Fig. 13) when it was assumed that all structural members that were, somehow, cut by the rock tip, undergo a combination of tearing and membrane tension collapse modes (Table 13). Bearing the above in mind, a combination of tearing and membrane tension collapse modes

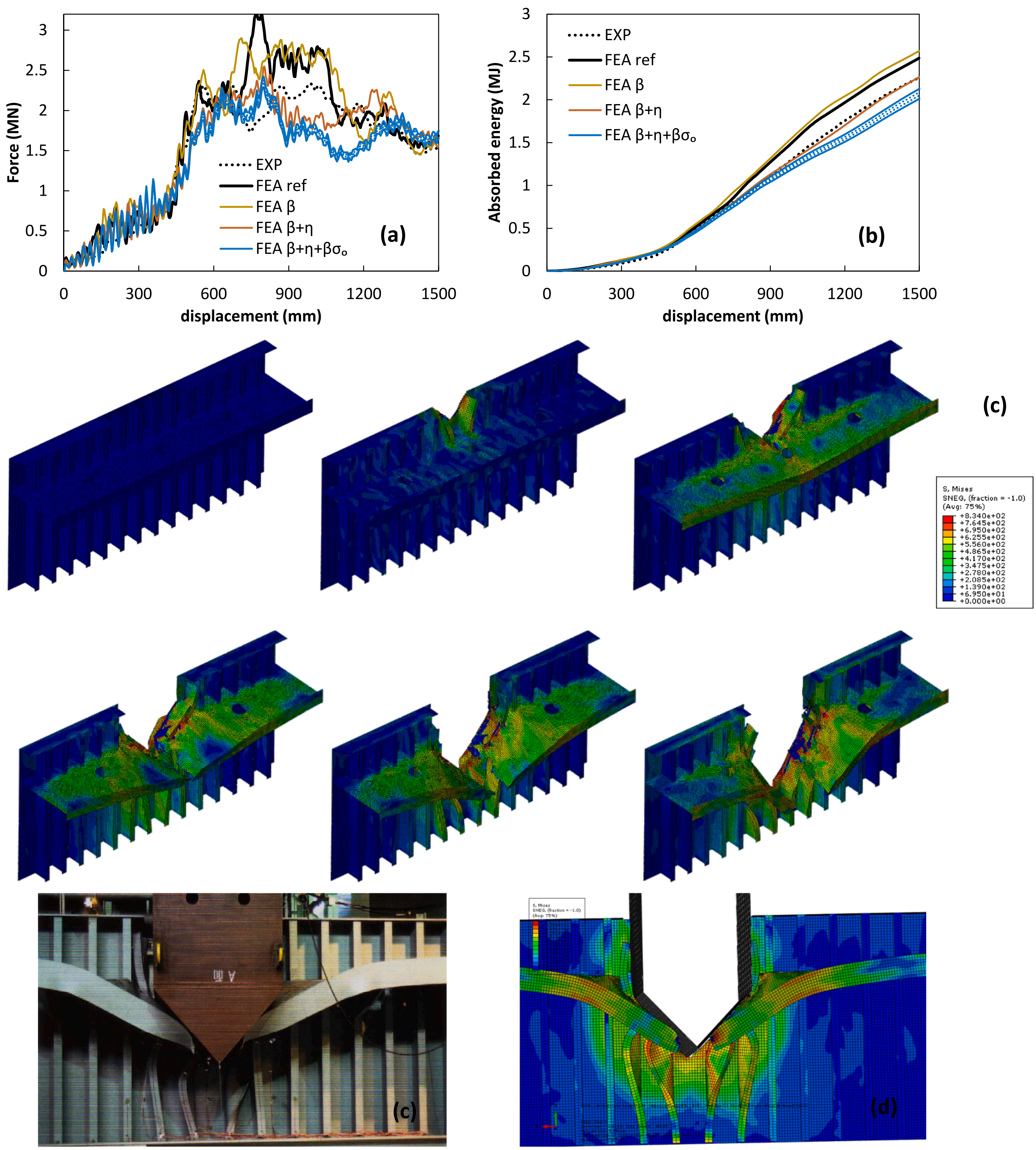

Fig. 10. Numerical modeling of raking test of ship bottom structure: a) reaction force responses of real-scale and miniature tests, b) absorbed energy response of real-scale and miniature tests, c) collapse evolution of the miniature FEA β+η+βσ0 model, d-e) torn ship bottom structure obtained from experiment and miniature FEA β+η+$\beta_{\sigma0}$ model

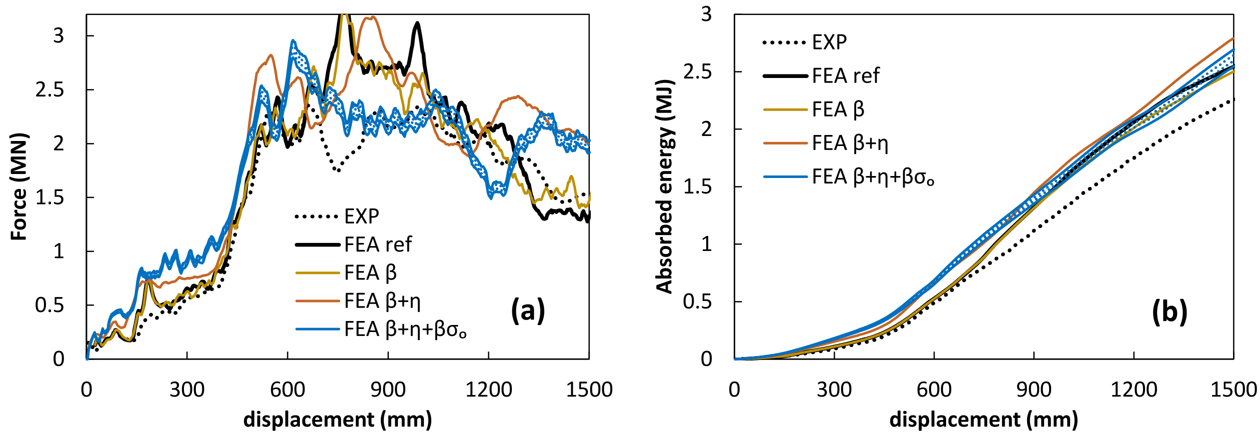

Fig. 11. Numerical modeling of raking test of ship bottom structure considering a failure criterion dependent on stress triaxiality: a) reaction force responses of real-scale and miniature tests, b) absorbed energy response of real-scale and miniature tests

was selected for both outer and inner shells as well as the transversal webs and bulkheads. The collapse mode for the rest of the structural members was considered to be folding in view of their structural collapse mode observed in the experiment. In the end, when comparing FEA ref and FEA β+η+βσ0 models, a reasonable agreement is observed in terms of the grounding horizontal force response (NRMSE = 6.98%) and the absorbed energy response (NRMSE = 6.86%).

5. Discussion of results

In this work, the effectiveness of the similarity technique to reproduce the collapse of large-scale marine structures in miniature when subjected to collision or grounding events presented in past works (Calle et al., 2020, Calle et al., 2020) was here numerically verified.

In order to do that, various experimental tests of large-scale marine structures found in literature were FE modeled in miniature to evaluate separately the accumulative effects of the size reduction (FEA β), size reduction and thickness distortion (FEA β+η) and size reduction, thickness distortion and material distortion (FEA β+η+βσ0) on the general structural response (force response and absorbed energy capability). Each experimental reference used for the analysis was here organized in study cases.

5.1. Examination of study cases

Some study cases presented significative discrepancies between experiment and FE reference model responses. This is because some particular characteristics of the experiments were not properly modeled by the simplified FE strategy used in this work due to two main reasons: limitations of the selected FE model and the lack of complementary information about the experiment. For these reasons, the numerical modeling of the experiment in real scale (FEA ref) is used as reference for comparative purpose in each study case while the experiment (EXP) is barely used as a starting point.

In general, it was observed that a perfect size reduction of the structure (FEA β) produces a nearly identical structural response when compared against that obtained by the real scale model (FEA ref) once brought to the same scale size using traditional similarity laws (Calle et al., 2020; Barenblatt, 2003).

On the other hand, the application of the thickness distortion in the models (FEA β+η) induced slight deviations in the structural response when compared against the reference model (FEA ref) in nearly all study cases carried out in this work (all except study cases #3 and #9). So far, it could be identified three main factors that determine these deviations when using thickness distortion related basically to: alteration of collapse mode, alteration of rupturing progress and lack of accuracy of FE modeling as better described below.

The collapse modes of some structures are more prone than others to alterations depending on their geometries. For instance, a specific buckling shape of a cylindrical shell structure subjected to axial compression is sensitive to its plate thickness (study case #5). In real structures, the buckling shape is also sensitive to diverse other factors such minor geometrical imperfections, residual stresses, eccentricity deviations in the force application point, etc. The analysis of an alternative model with a preset warping in the external shell ended up fostering a global collapse mode closer to the experimental real-size reference, but at the cost of a decrease in the force level. Besides, to avoid lack of accuracy with respect to collapse/buckling appearance, less drastic scale reductions should be employed as verified by the second alternative model. The collapse mode of the second alternative model showed to be quite identical to the real-scale structure using a moderate reduction scale of 1:15. On the other hand, the buckling shape of a conical shell body is less affected by these factors because its own geometry fosters a determined folding pattern as clearly seen in study cases #4.

Also, when thickness distortion is adopted, some structures showed to be particularly prone to bear alterations in rupturing progress. In other words, in spite of the structural members be consistent with their reference structural collapse modes, the crack initiation occurs a little later as observed in the study cases #1, #2, #6 and #8. Particularly, these study cases involved the rupture of plates that underwent membrane tension and tearing. A contrary effect (earlier occurrence of crack initiation) was also observed when changing material from an A-grade shipbuilding steel to a 316L austenitic steel. In most of the cases, both

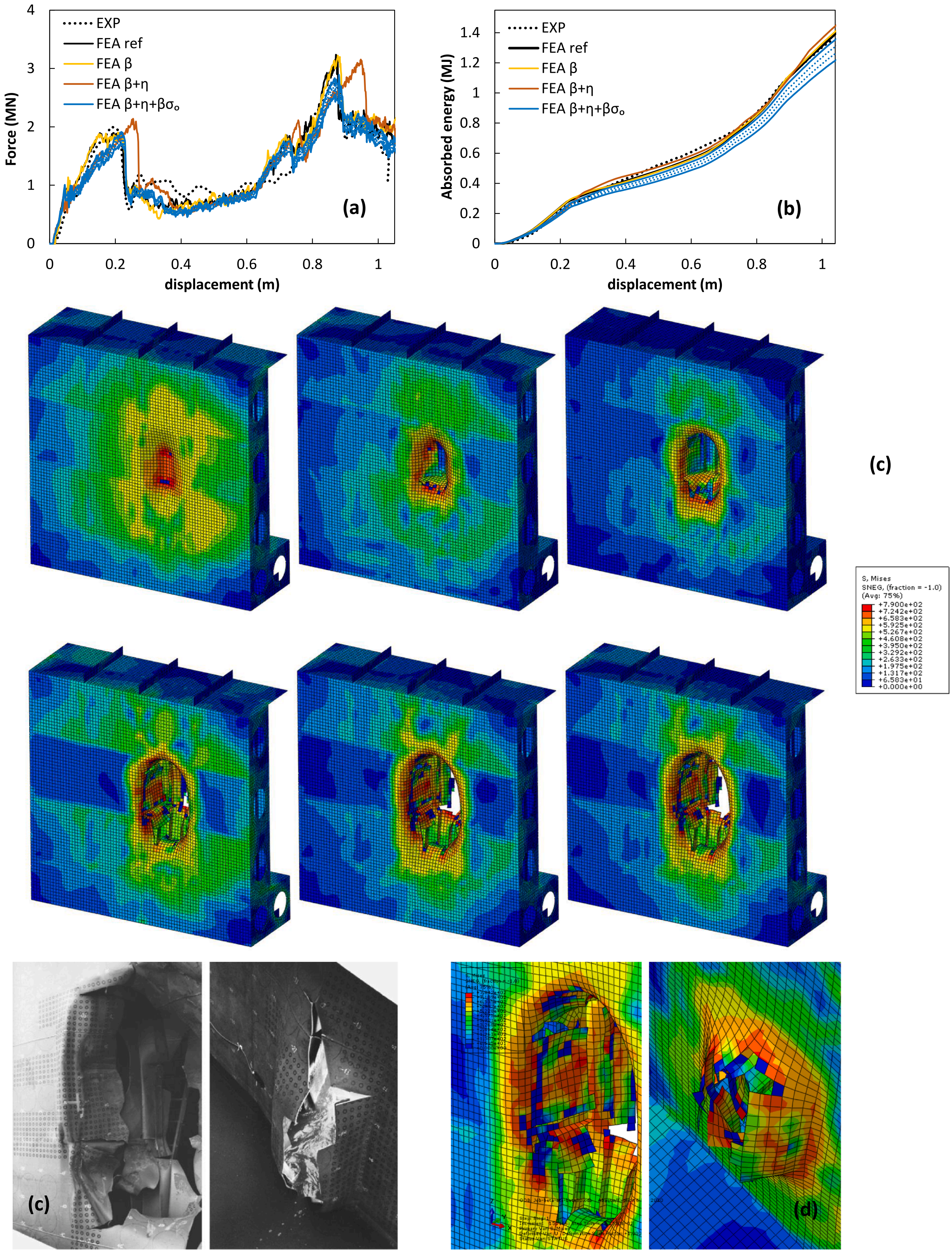

Fig. 12. Numerical modeling of ship collision large-scale test: a) reaction force responses of real-scale and miniature tests, b) absorbed energy responses of real-scale and miniature tests, c) collapse evolution of the miniature FEA β+η+βσ0 model, d-e) collapsed configurations of outer and inner shell structures obtained from experiment and miniature FEA β+η+$\beta_{\sigma 0}$ model

Table 12
Evaluation of nominal thicknesses for individual structural members of miniature hull structures.

Structural member	Dominant collapse mode	Prototype thickness FEA ref (mm)	YS [FS1] (MPa)	UTS (MPa)	Average [FS2] (MPa)	FS ratio	Thickness distortion factor	Model thickness FEA β (mm)	Failure strain FEA ref FEA β	Model thickness FEA β+η (mm)	Failure strain FEA β+η	Model thickness FEA β+η+βσ$_0$ (mm)	Failure strain FEA β+η+βσ$_0$
Outer shell	Tearing and Membrane	5.0	314	460	387	1.0	4.605	0.2	0.166	0.679	0.232	0.679	0.232
Inner shell	Tearing and Membrane	5.0	314	460	387	1.0	4.605	0.2	0.166	0.679	0.232	0.679	0.232
Stiffening flat bars	Folding	5.0	314	460	387	1.0	2.5	0.2	0.169	0.5	0.219	0.5	0.219
Vertical web	Folding	6.0	314	460	387	1.0	2.5	0.24	0.176	0.6	0.226	0.6	0.226
Horizontal stringer	Folding	5.0	314	460	387	1.0	2.5	0.2	0.165	0.5	0.215	0.5	0.215

opposite effects compensate each other so resulting in a good correspondence in terms of absorbed energy (as seen in study cases #1, #6 and #8).

It is worth mentioning that the lack of accuracy of a simplified FE modeling ended up affecting the resulting structural response when thickness or material are changed. An example of this are experiments that involved interaction with sharp indenters (study cases #2 and #7) that would need to employ a refined mesh in the contact areas to enhance the structural response accuracy for comparative purpose. Other example is related to the failure criterion. A simple failure criterion based on maximum plastic strain with sensitivity to element-length-to-thickness ratio was adopted in this research, but, sometimes, this criterion can be very imprecise when material failure strongly depends on the stress triaxiality (see study case #3 and #7), particularly to deal with a combination of membrane tension and tearing modes as evidenced in Ref. (Calle et al., 2019). This numerical limitation can be evidenced when errors in force and energy responses are reduced when implementing stress triaxiality-based failure criteria (with material parameters extracted from mild steel (Calle et al., 2019)) to reevaluate models of study cases #3 and #7 (Figs. 4 and 11). However, these reevaluated models can be only used to give an idea of the numerical shortcomings, but stress triaxiality-based failure criteria cannot be implemented in all nine study cases since most of these cases lacks in appropriate experimental testing and materials data (Calle and Alves, 2015) to be able to evaluate the criteria parameters.

5.2. Selection of collapse mode

As previously mentioned, the similarity technique involves an increase of the thickness of structural members to make they all able to build by AM. The evaluation of the thickness distortion is individual for each structural member according to its expected collapse mode. In this work, the selection of each collapse mode was aided with the available data of the experiment.

However, this technique aims to predict experimentally the structural response in testing configurations without necessarily having a previous experimental reference. It is worth mentioning that the choice of an erroneous collapse mode, for a specific structural member, leads to a different thickness distortion and that consequently results in a structural response different from that expected. Sometimes this choice is obvious, sometimes it is not. In this sense, it is strongly suggested a preliminary numerical analysis to select correctly the collapse mode of each structural part.

On the other hand, the set of study cases evaluated in this work permitted to gain a better understanding of how the collapse modes are induced in each structural member and some considerations can be made.

For instance, the study cases let evident that the tearing mode is difficult to occur unless under specific conditions such as when a sharp rigid indenter cuts laterally a plate structure as seen in study case #7. However, when modeling a typical tearing collapse that results from a ship grounding event (study case #9), it was verified that it is necessary to take into account the overlapping of the tearing and membrane tension collapse modes. Once the inner and outer plates of marine structures stretched both perpendicularly and laterally by a rigid obstacle, a large amount of plastic stretching occurs before and simultaneously with the tearing of the plates. At the same time, a combination of membrane tension and tearing represents better the structural collapse of a collided double-plate hull (study case #8) that undergoes membrane tension in a first stage and, once the crack is initiated, the most relevant collapse mode becomes tearing as long as the crack is being opened.

However, sometimes, the overlapping of collapse modes occurs temporarily and quickly as seen in the web girder test described in the study case #6. In the beginning of the contact, the stringer deck is vertically compressed so achieving an instable peak force that suddenly fall when it starts to fold. But, when its thickness is increased, the stringer deck gets more stable to vertical compression so achieving a higher peak force before it starts to fold. In spite of that, the stringer deck cannot consider a combination of collapse modes because the compression stage is very short and less relevant for plates when compared against the folding response.

6. Conclusions

A structural similarity technique for experimental modeling of ship collision, grounding and similar events via miniature models with drastic scale reduction (50 to 100 times reductions) was here investigated through numerical analyses and revised. The revision of the similarity technique involved the definition of new combined collapse modes and the redefinition of the flow stress concept.

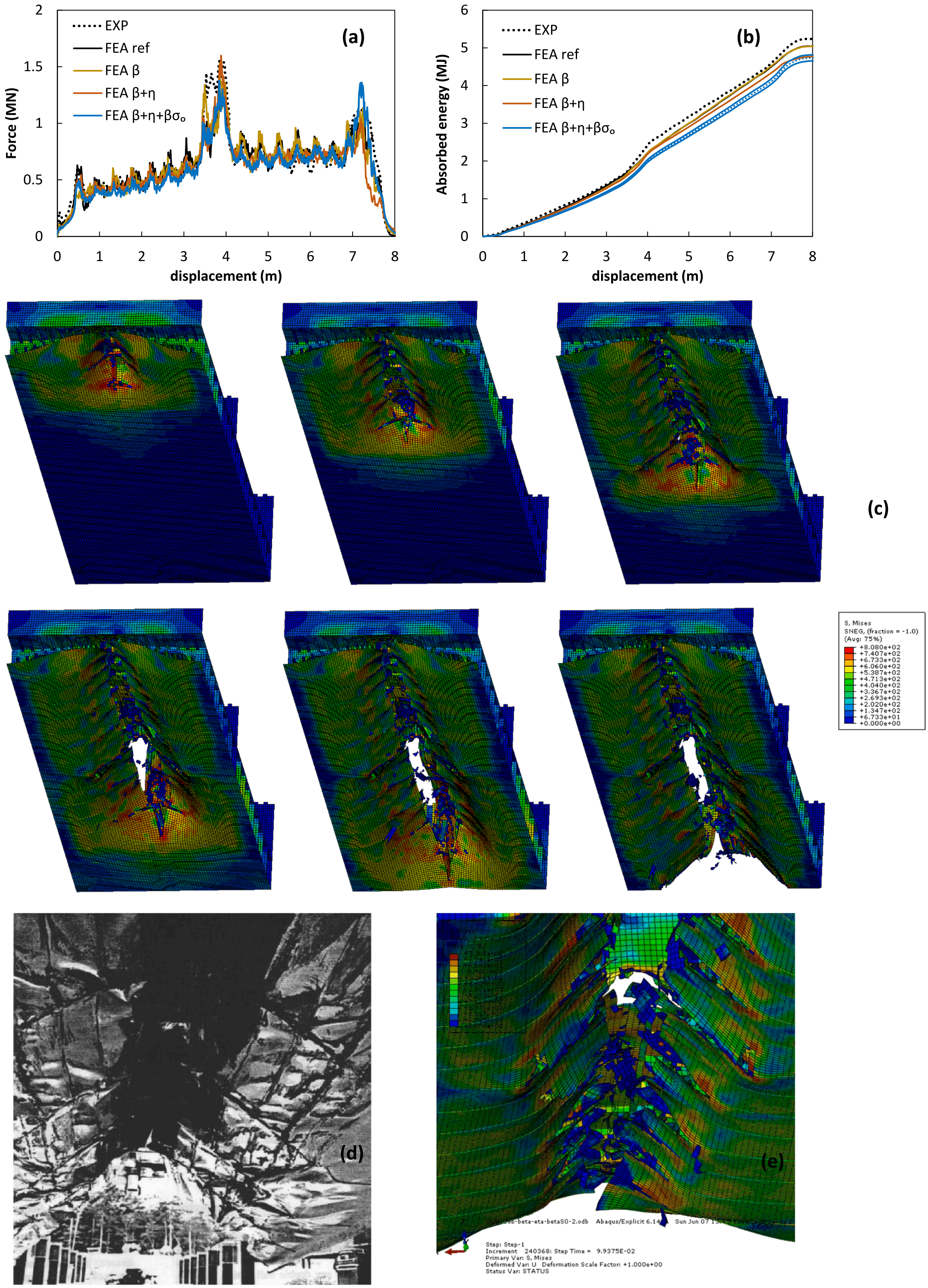

Fig. 13. Numerical modeling of grounding test of ship bottom structure: a) horizontal reaction force responses in rock tip of real-scale and miniature tests, b) absorbed energy responses of real-scale and miniature tests, c) collapse evolution of the miniature FEA β+η+βσ0 model, d-e) torn ship bottom structure obtained from experiment and miniature FEA $\beta+\eta+\beta_{\sigma 0}$ model

Table 13
Evaluation of nominal thicknesses for individual structural members of miniature ship bottom structures.

Structural member	Dominant collapse mode	Prototype thickness FEA ref (mm)	YS [FS1] (MPa)	UTS (MPa)	Average [FS2] (MPa)	FS ratio	Thickness distortion factor	Model thickness FEA β (mm)	Failure strain FEA ref FEA β	Model thickness FEA β+η (mm)	Failure strain FEA β+η	Model thickness FEA β+η+βσ$_0$ (mm)	Failure strain FEA β+η+βσ$_0$
Outer shell	Tearing and Membrane	3.13	283	345	314	1.0	5.314	0.157	0.170	0.832	0.258	0.832	0.258
Inner shell	Tearing and Membrane	3.13	283	345	314	1.0	5.314	0.157	0.170	0.832	0.258	0.832	0.258
Longitudinal web	Folding	2.28	283	345	314	1.0	3.5	0.114	0.153	0.399	0.219	0.399	0.219
Transversal web	Tearing and Membrane	1.90	283	345	314	1.0	5.314	0.095	0.144	0.505	0.232	0.505	0.232
Transversal bulkhead	Tearing and Membrane	3.13	283	345	314	1.0	5.314	0.157	0.170	0.832	0.258	0.832	0.258
Bulkhead stiffener	Folding	3.13	283	345	314	1.0	3.5	0.157	0.170	0.548	0.236	0.548	0.236
Outer shell stiffener	Folding	2.28	283	345	314	1.0	3.5	0.114	0.153	0.399	0.219	0.399	0.219
Inner shell stiffener	Folding	3.51	283	345	314	1.0	3.5	0.176	0.176	0.614	0.242	0.614	0.242
Reinforcing rings	Folding	4.57	283	345	314	1.0	3.5	0.229	0.190	0.800	0.256	0.800	0.256

The main shortcoming of the similarity technique with thickness distortion was the selection of barely one of the most relevant collapse modes for each structural member. It is worth mentioning that some of the structural members are subjected simultaneously or sequentially to two collapse modes in different proportions and different moments: membrane tension and tearing ($\eta_{t,m+t}$) and membrane tension and folding ($\eta_{t,m+f}$). The selection of one collapse mode implies the exclusion of the other. This exclusion, in most of the cases, lead to significant similarity errors depending on the thickness distortion factor, for example: membrane tension or folding leads to a difference of $\eta^{2/3}$ ($= \eta^{5/3} - \eta$) while membrane tension or tearing leads to $\eta^{5/9}$ ($= \eta^{5/3} - \eta^{10/9}$). By considering two combined collapse modes, a compromise approach is achieved and similarity errors from the exclusion of one of them are then minimized.

Another goal of this work was the redefinition of the flow stress, not by taking into account the whole shape of the stress-strain curve, but laying greater emphasis to the plastic straining (which is more associated to the material collapse). This emphasis is attained by considering the portions of the true stress-strain curves in full plastic deformation for both materials (prototype and model), i.e., right in the middle of the stress-strain curve before necking occurrence. This redefinition came with a reduction in similarity errors caused by large discrepancies in the overall shape of the stress-strain curves of prototype and model materials (when comparing the range from yield stress to ultimate tensile strength) once they are now compared in a more focused full plastic regime.

The numerical analysis comprised the evaluation of nine study cases in which destructive tests performed in large-scale marine structures were reproduced in reduced scale. With all these amendments in the similarity technique, in general, it was possible to obtain numerically a reasonable correspondence between the prototypes (reference large-scale structures) and the models (miniature structures) in terms of reaction force and absorbed energy responses. This agreement can be easier observed in more complex structures with a large quantity of structural members such as the ship collision and grounding tests also modeled here.

As a limitation, the similarity technique also revealed to be prone to fail reproducing the exact buckling collapse of some particular geometries that showed, to some extent, sensitivity to thickness distortion. This limitation is amended when using less drastic scale reductions as in the case of evaluating the structural performance of partial structures. Besides, some miniature structural members subjected to pure and combined membrane tension also presented some divergences related to early or late crack initiation induced by the thickness distortion and material distortion respectively.

In this sense, future works aim to focus dealing with these limitations through geometrical alterations of the models, numerical analyses and, especially, experimental miniature tests. Finally, the aim of next studies is to verify the accuracy of this experimental modeling tool and to simulate more complex ship collision and grounding events which are challenging to reproduce numerically using finite element method.

CRediT authorship contribution statement

Miguel Angel Calle Gonzales: Conceptualization, Methodology, Investigation, Data curtion, Writing – original draft, Writing – review & editing. **Pentti Kujala:** Conceptualization, Supervision, Writing – review & editing, Resources, Project administration, Funding acquisition.

Declaration of Competing Interest

The authors declare that they have no known competing financial interests or personal relationships that could have appeared to influence the work reported in this paper.

Acknowledgments

The leading author acknowledges the support of the Marine Technology Research Group of Aalto University while working there.

Supplementary materials

Supplementary material associated with this article can be found, in the online version, at doi:10.1016/j.apor.2021.102653.

Appendix. Normalized root mean square error (NRMSE) formulae

NRMSE for structural reaction force response

$$\mathrm{NRMSE} = \frac{1}{\left|F_{ref}^{max} - F_{ref}^{min}\right|}\sqrt{\frac{\sum_{i=1}^{N}\left(F_{ref,i} - F_{\beta+\eta+\beta_{\sigma0},i}\right)^2}{N}}$$

where $F_{ref,i}$ and $F_{\beta+\eta+\beta_{\sigma0},i}$ are the reaction forces at point i in the reference model (FEA ref) and in the reduced scale model with thickness and material distortions (FEA $\beta+\eta+\beta\sigma_0$), respectively, once brought to the same dimensional scale; N is the sample size; F_{ref}^{max} and F_{ref}^{min} are the maximum and minimum force values obtained from the FEA ref model; $F_{\beta+\eta+\beta_{\sigma0}}$ is evaluated as the average of its upper and lower bounds.

NRMSE for structural absorbed energy response

$$\mathrm{NRMSE} = \frac{1}{\left|E_{ref}^{max} - E_{ref}^{min}\right|}\sqrt{\frac{\sum_{i=1}^{N}\left(E_{ref,i} - E_{\beta+\eta+\beta_{\sigma0},i}\right)^2}{N}}$$

where $E_{ref,i}$ and $E_{\beta+\eta+\beta_{\sigma0},i}$ are the absorbed energies at point i in the reference model (FEA ref) and in the reduced scale model with thickness and material distortions (FEA $\beta+\eta+\beta\sigma_0$), respectively, once brought to the same dimensional scale; N is the sample size; E_{ref}^{max} and E_{ref}^{min} are the maximum and minimum absorbed energy values obtained from the FEA ref model; $E_{\beta+\eta+\beta_{\sigma0}}$ is evaluated as the average of its upper and lower bounds.

References

Barenblatt, G.I., 2003. Scaling. Cambridge University Press.
Calle, M.A.G., Alves, M., 2015. A review-analysis on material failure modeling in ship collision. Ocean Eng. 106, 20–38, 9.
Calle, M.A.G., Kujala, P., 2019. 3D printing miniature marine structures models for structural analysis purpose: is it possible? Volume 3: Structures, Safety, and Reliability.
Calle, M.A.G., Oshiro, R.E., Alves, M., 2017. Ship collision and grounding: scaled experiments and numerical analysis. Int. J. Impact Eng. 103, 195–210, 5.
Calle, M.A.G., Oshiro, R.E., Kõrgesaar, M., Alves, M., Kujala, P., 2019. Combined strain rate, mesh size and calibration test influence on structural failure: miniature ship grounding test. Ocean Eng. 173, 215–226, 2.
Calle, M.A.G., Salmi, M., Mazzariol, L.M., Alves, M., Kujala, P., 2020. Additive manufacturing of miniature marine structures for crashworthiness verification: scaling technique and experimental tests. Mar. Struct. 72, 102764, 7.
Calle, M.A.G., Salmi, M., Mazzariol, L.M., Kujala, P., 2020. Miniature reproduction of raking tests on marine structure: similarity technique and experiment. Eng. Struct. 212, 110527, 6.
Endo, H., Yamada, Y., Kitamura, O., Suzuki, K., 2002. Model test on the collapse strength of the buffer bow structures. Mar. struct. 15, 365–381, 7.
Kaminski, M., Rigo, P., 2018. Proceedings of the 20th International Ship and Offshore Structures Congress (ISSC 2018) - Specialist Committee Reports. IOS Press, Amsterdam, Netherlands.
Karlsson, U., Ringsberg, J., Johnson, E., Hoseini, M., Ulfvarsson, A., 2009. Experimental and numerical investigation of bulb impact with a ship side-shell structure. Mar. Technol. 46, 16–26.
Kim, S.J., Kõrgersaar, M., Ahmadi, N., Taimuri, G., Kujala, P., Hirdaris, S., 2021. The influence of fluid structure interaction modelling on the dynamic response of ships subject to collision and grounding. Mar. struct. 75, 102875, 1.
Kõrgesaar, M., Romanoff, J., Remes, H., Palokangas, P., 2018. Experimental and numerical penetration response of laser-welded stiffened panels. Int. J. Impact Eng. 114, 78–92, 4.
Lehmann, E., Peschmann, J., 2002. Energy absorption by the steel structure of ships in the event of collisions. Mar. struct. 15, 429–441, 7.
Liu, B., Pedersen, P.T., Zhu, L., Zhang, S., 2018. Review of experiments and calculation procedures for ship collision and grounding damage. Mar. struct. 59, 105–121, 5.
Liu, B., Soares, C.G., 2016. Assessment of the strength of double-hull tanker side structures in minor ship collisions. Eng. Struct. 120, 1–12, 8.
Liu, B., Villavicencio, R., Soares, C.G., 2015. Simplified analytical method to evaluate tanker side panels during minor collision incidents. Int. J. Impact Eng. 78, 20–33, 4.
Liu, Y.L., Zhang, A.M., Tian, Z.L., Wang, S.P., 2018. Numerical investigation on global responses of surface ship subjected to underwater explosion in waves. Ocean Eng. 161, 277–290, 8.
Marinatos, J.N., Samuelides, M.S., 2015. Towards a unified methodology for the simulation of rupture in collision and grounding of ships. Mar. struct. 42, 1–32, 7.
Martens, I., 2014. Konstruktive Aspekte beim Entwurf von Bugwülsten zur Verbesserung des Energieaufnahmevermögens bei Schiffskollisionen. TUHH Universitätsbibliothek.
Mazzariol, L.M., Oshiro, R.E., Alves, M., 2016. A method to represent impacted structures using scaled models made of different materials. Int. J. Impact Eng. 90, 81–94, 4.
Ohtsubo, H., Kawamoto, Y., Kuroiwa, T., 1994. Experimental and numerical research on ship collision and grounding of oil tankers. Nucl. Eng. Des. 150, 385–396, 9.
Oshiro, R.E., Calle, M.A.G., Mazzariol, L.M., Alves, M., 2017. Experimental study of collision in scaled naval structures. Int. J. Impact Eng. 110, 149–161, 12.
Peschmann, J., 2001. Berechnung der Energieabsorption der Stahlstruktur von Schiffen bei Kollision und Grundberührung. Maritime Archive, Delft.
Qiankun, J., Gangyi, D., 2011. A finite element analysis of ship sections subjected to underwater explosion. Int. J. Impact Eng. 38, 558–566, 7.
Ringsberg, J.W., Amdahl, J., Chen, B.Q., Cho, S.-R., Ehlers, S., Hu, Z., Kubiczek, J.M., Kõrgesaar, M., Liu, B., Marinatos, J.N., Niklas, K., Parunov, J., Quinton, B.W.T., Rudan, S., Samuelides, M., Soares, C.G., Tabri, K., Villavicencio, R., Yamada, Y., Yu, Z., Zhang, S., 2018. MARSTRUCT benchmark study on nonlinear FE simulation of an experiment of an indenter impact with a ship side-shell structure. Mar. Struct. 59, 142–157, 5.
Rodd, J., 1996. Observations on conventional and advanced double hull grounding. In: Int. Conf. on Designs and Methodologies for Collision and Grounding. San Francisco.
Simonsen, B.C., 1997. Ship grounding on rock—II. Validation and application. Mar. struct. 10, 563–584, 8.
Simonsen, B.C., 1997. Mechanics of Ship Grounding. Technical University of Denmark.
Smith, M., 2009. ABAQUS/Standard User's Manual, Version 6.9. Dassault Systèmes Simulia Corp, United States.

Soares, C.G., Garbatov, Y., 2015. Proceedings of the 19th International Ship and Offshore Structures Congress (ISSC2015) - Specialist Committee Reports. The: CRC Press/ Balkema, Leiden.

Tautz, I., Schöttelndreyer, M., Lehmann, E., Fricke, W., 2010. Schiffskollisionen im quasi-statischen Versuch. In: ANSYS Conference & 29th CADFEM User's Meeting.

Törnqvist, R., 2003. Design of crashworthy ship structures. Technical University of Denmark, Department of Mechanical Engineerning, Maritime Engineering, Kgs. Lyngby.

Yamada, Y., 2007. Buffer bulbous bows: a measure to reduce oil spill in collisions. DTU.

Yamada, Y., Pedersen, P., 2008. A benchmark study of procedures for analysis of axial crushing of bulbous bows. Mar. Struct. 21, 257–293, 4.

Zhang, A., Suzuki, K., 2007. A comparative study of numerical simulations for fluid–structure interaction of liquid-filled tank during ship collision. Ocean Eng. 34, 645–652, 4.

Zhang, S., Villavicencio, R., Zhu, L., Pedersen, P.T., 2019. Ship collision damage assessment and validation with experiments and numerical simulations. Mar. struct. 63, 239–256, 1.